TECHNISCHE UNIVERSITÄT WIEN

VIENNA UNIVERSITY OF TECHNOLOGY

DIPLOMARBEIT

Transient One-Dimensional Fluid Flow in High Pressure Applications for Diesel-Fuel

ausgeführt am Institut für
Strömungsmechanik und Wärmeübertragung
der Technischen Universität Wien

unter der Anleitung von
Ao.Univ.Prof. Dipl.-Ing. Mag.rer.nat. Dr.techn. Herbert Steinrück

durch

Johannes Srajer
Diefenbachgasse 45-47/2/8
1150 Wien

Wien, am 27. Juli 2010

Acknowledgment

Initially I would like to thank Prof. Herbert Steinrück and Dr. Harald Schmidt for proposing and supervising this work. I also thank the whole Team from the ECS-MES department for their constant support, especially Christof, Alexander and Andreas. I would further like to thank my colleges form the institute of fluid dynamics for helping me with the numerical implementation. I deeply thank my family and friends, without their constant support my studies and this work would not have been possible. My special thanks go to Julia who permanently supports me. This work is for you!

This work was partially financed by Magna Powertrain and the technical University of Vienna.

Abstract

Future emission laws like $EURO\ VI$, $JPNLT$, US 10 and $US\ T4$ require to increase the efficiency of diesel engines. Shaping the rate of diesel fuel injected into a cylinder during one combustion cycle has great influence on emission of CO, NO_x and *sooty particles*. In order to determine an optimal rate shaping, knowledge of the thermodynamic behavior of diesel and of the pressure waves in the components of the injection system is needed.
Here we deduce a simulation model, that calculates transient one-dimensional flow of diesel fuel. The model consists of three components, which are all based on the equations of state for liquid diesel fuel. The flow in the pipes is considered one-dimensional and inviscid. Thus the Euler equations are solved numerically using Roe's method. In a volume the kinetic energy can be neglected and the changes of internal energy are calculated by a mass and energy balance considering the in and outflow masses and their enthalpy and the change of volume with time, as well. A throttle will be described by a pressure loss coefficient. Changes of temperature due to the Joule-Thomson effect are also taken into account. Equations of state for liquid diesel Fuel have been derived from measured data for density and isobaric heat capacity. The equation of state is tested by comparing the predicted values for the speed of sound with measured data reported in the literature. To proof the ability of the simulation tool to resolve shock and rarefaction waves as well as contact discontinuities, the results for a shock tube test are shown. Further the change of density and temperature during compression and expansion in a piston pump is shown. Also the results for two volumes with different initial conditions, connected by a throttle in one test case and connected by a pipe in another test case, show different transient behavior. This work shall help simulating transient one dimensional flow of liquid diesel fuel in modern diesel injection systems, having operating pressures of up to 2500 bar and operating temperatures from 260 K to 393 K.

Kurzdarstellung

Künftige Abgasnormen wie $EURO\,VI$, $JPNLT$, $US10$ und $US\,T4$ erfordern eine Steigerung der Effizienz von Dieselmotoren. Der Verlauf der Einspritzrate des Dieselkraftstoffes während eines Brennzyklus spielt eine entscheidende Rolle für die Emission von CO, NO_x und $Russpartikeln$. Um optimale Einspritzverlaufs- Formung zu bestimmen, bedarf es sowohl einer genauen Kenntnis der thermodynamischen Eigenschaften des Dieselkraftstoffes, als auch der sich ausbreitenden Wellen in den einzelnen Komponenten.
Hier wird eine Simulationsmodell abgeleitet, das instationäre eindimensionale Strömungsvorgänge von Dieselkraftstoff berechnet. Das Modell besteht aus drei Komponenten, deren gemeinsame Grundlage eine Zustandsgleichung für flüssigen Dieselkraftstoff ist. Die Strömung in den Rohrleitungen wird eindimensional und reibunsfrei angenommen. Daher werden die Euler Gleichungen numerisch, mittels der Methode von Roe, gelöst. In einem Vorratsbehälter (Volumen) können die kinetischen Energien vernachlässigt und die Änderungen der inneren Energie mittels Massen- und Energiebilanz berechnet werden, unter Berücksichtigung von ein- und ausströmender Masse und Enthalpie, sowie der zeitlichen Änderung des Gesamtvolumens. Drosseln werden durch Druckverlustbeiwerte beschrieben. Außerdem werden Änderungen der Temperatur aufgrund des Joule-Thomson Effekts berücksichtigt. Die benötigten Zustandsgleichungen für flüssigen Diesel Kraftstoff werden aus Messungen von Dichte und isobarer Wärmekapazität hergeleitet. Um diese Zustandsgleichung zu testen, wurden daraus berechnete Werte für die Schallgeschwindigkeit mit Werten aus der Literatur verglichen. Um das Simulationsmodell auf die Fähigkeit Druckwellen, Verdünnungsfächer und Kontaktunstetigkeiten auflösen zu können zu überprüfen, werden die Ergebnisse eines Stoßrohrproblems gezeigt. Weiters werden die Änderungen von Dichte und Temperatur während der Kompression und Expansion in einer Kolbenpumpe gezeigt. Außerdem wurden zwei verschiedene Kombinationen von Komponenten ausgetestet. Zwei Volumina mit unterschiedlichen Anfangsbedingungen werden in einem Test mit einer Drossel und in einem anderen Test mit einer Leitung verbunden. Der zeitliche Verlauf der daraus resultierenden Ausgleichsvorgänge wird gezeigt.
Die Arbeit soll helfen instationäre eindimensionale Strömungsvorgänge von flüssigem Diesel in modernen Einspritzsystemen, mit Betriebsdrücken bis zu 2500 bar und Temperaturen zwischen $-10°$ C und $120°$ C, zu simulieren.

Contents

List of Figures

List of Tables

Chapter 1

Introduction

To simulate procedures in injection systems of diesel fuel engines interdisciplinary methods from the fields of fluid mechanics, technical mechanics, electrical engineering and automatic control engineering have to be used. The numerical simulation of injection systems plays an important role for developing and dimensioning new components. Considerable requirements for the quality of the model and the numerics behind, are resulting out of high pressures used, and out of the little amount of fuel that gets injected during each combustion cycle ($\approx 1.5\ mm^3 \pm 0.5\ mm^3$). Furthermore it must be pointed out that fuel injection is a transient phenomenon, that can stimulate strong oscillations in valves and other components, and that can cause mechanical stress resulting in cavitation damage [Mollenhauer, 2002]. Also notable heating of the fuel due to throttle and friction losses, with extensive impact on the characteristics of the fuel, have to be quantified. New emission legislation boosts the need for new solutions. In order to comply with emission laws like EURO VI, JPNLT, US 10 and US T4, manufacturer need to reduce the emission of CO, NO_x and *sooty particles* [Parche, 2010]. Therefore a wide variety of solutions within the engine, exhaust gas aftertreatment, air and injection systems have been taken into account. It was shown that continuous rate shaping during the injection helps not only reducing emissions and therefore reducing fuel consumption, but also helps reducing the noise of the engine, which is also one of the main goals in designing new diesel engines. To investigate effects of rate shaping turns out to be a very powerful tool for developing better engines [Predelli, 2010].

To understand what is behind rate shaping one needs to understand the fuel cycle, which is indicated by the yellow closed loop in figure 1.1 [BMW, 2006]. The fuel cycle in a diesel engine starts in the tank where the fuel is stored under atmospheric pressure. An electrical lift pump transports the fuel to the low pressure pump (LPP), where the pressure increases up to a few bars. From there on the fuel is forced through a filter first, before it gets to the high pressure pump (HPP). In the high pressure pump the fuel gets compressed to a pressure up to 2200 *bar* (in the future up to 2500 *bar*), depending on the manufacturer of the injection system [Leonhard, 2009]. The highly pressurized fuel is then conducted to the so called rail, which is a high pressure fuel reservoir, as well as to the pressure control valve (PCV), at the end of the rail, and to the

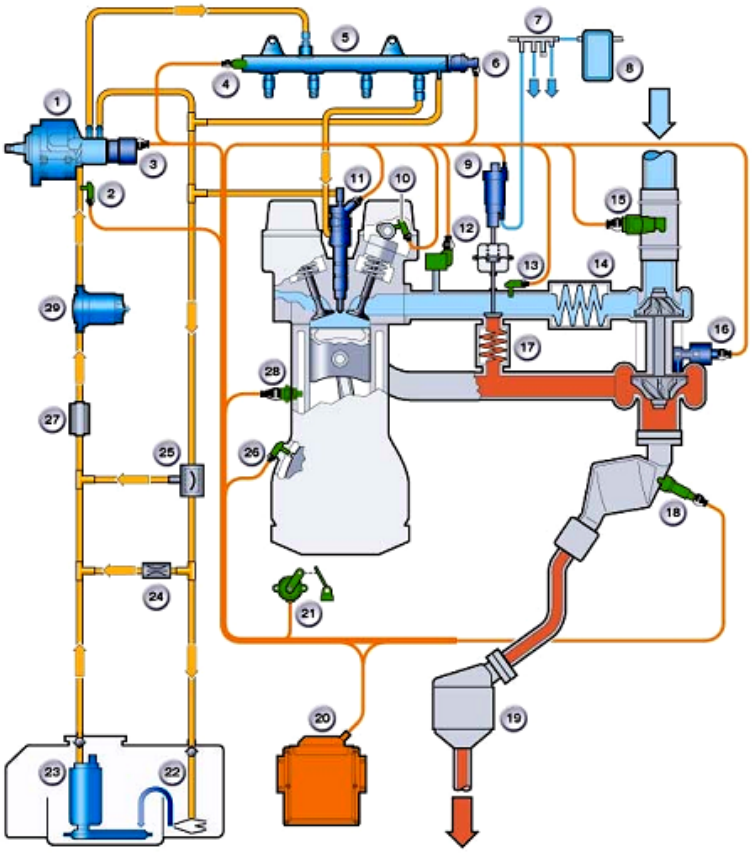

Figure 1.1: Common Rail Scheme containing the fuel cycle (yellow), control unit cycle (orange), intake and exhaust air cycle (blue and red). Components: 1. HPP, 2. fuel heat sensor, 3. suction control valve, 4. rail pressure sensor, 5. rail, 6. PCV, 7. low pressure manifold, 8. low pressure reservoir, 9. pressure converter, 10. camshaft pickup, 11. injector, 12. + 13. + 15. charge air sensors, 14. charge-air intercooler, 16. variable nozzle turbine actuator, 17. exhaust gas recirculation inter-cooler, 18. lambda sensor, 19. exhaust silencer, 20. control unit, 21. gas pedal module, 22. tank, 23. electrical pump, 24. return flow throttle, 25. bimetal valve, 26. crank shaft pickup, 27. LPP, 28. coolant sensor, 29. filter

injector itself, for activation piloting. Through high pressure pipes the fuel gets conducted from the rail to the injectors, which are installed on top of each cylinder of the engine. Since only a little amount of fuel is injected into the cylinder during one combustion, a major part of the fuel flows through the pressure control valve, which regulates the pressure in the rail, and through some other throttles, back into the tank, where the fuel cycle has started.

A variety of injectors are available on the market, using different technologies. To outline the function of an injector, one technology that is controlled by a magnetic valve (see figure 1.2 [BMW, 2006]) is presented here. Since the injector is connected to the rail via a pipe, the rail pressure is present at the inlet of the injector. Through a bore hole in the injector the fuel is transported down to a small reservoir storing pressurized fuel. Since the force from the injector spring together with the pressure from the activation piloting outweigh the force from the small

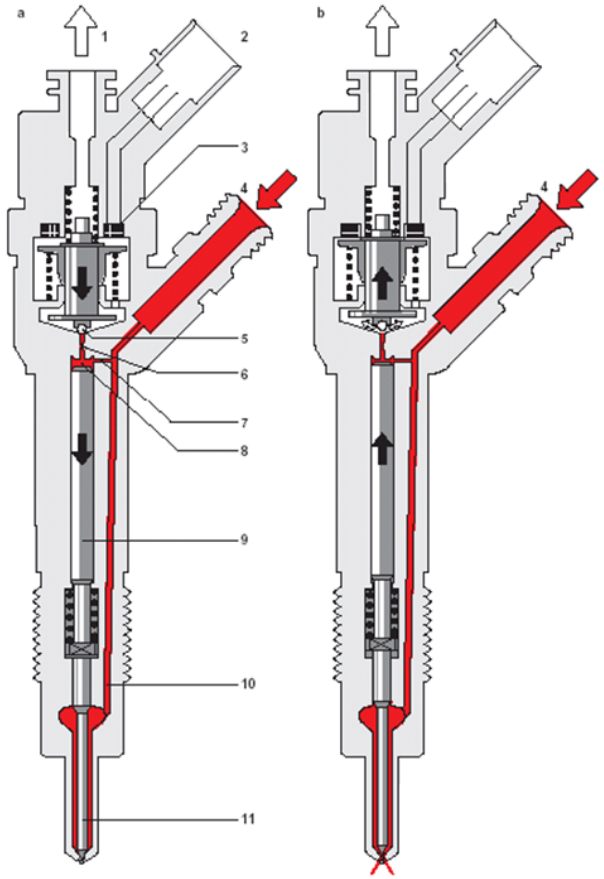

Figure 1.2: Schematic drawing of an injector with closed nozzle (a) and during injection with open nozzle (b). Components: 1. fuel return line, 2. electrical plug, 3. magnetic control device, 4. fuel intake (high pressure), 5. ball valve, 6. drain throttle, 7. inlet throttle, 8. valve control reservoir, 9. valve control piston, 10. nozzle inlet pipe, 11. needle

reservoir, the injector stays in a closed position. When the control device supplies the magnetic valve with an electric current the anchor lifts up and opens the ball valve. The pressure of the activation piloting drops, therefore the needle lifts up and opens the injector nozzle. After a certain amount of time the control device stops the electric current. Then the pressure at the activation piloting increases, since the ball valve closes again, and the needle is forced back closing the nozzle. Modern injectors use piezo stacks instead of the magnetic valve to lift the needle, because of shorter reaction times and therefore better control over the amount of fuel that gets injected.

What is called rate shaping is the technique of using a certain progression in the amount of fuel injected into the cylinder during one combustion cycle. Different types of rate shaping are actually in the focus of engine developers across the world, as for example the multiple injections (see figure 1.3) and also the continuous progressions of the rate injected into the cylinder.

In order to make a transient simulation of the whole fuel cycle, including all pumps, valves and pipes, one dimensional calculations deliver results within an appropriate expenditure of time.

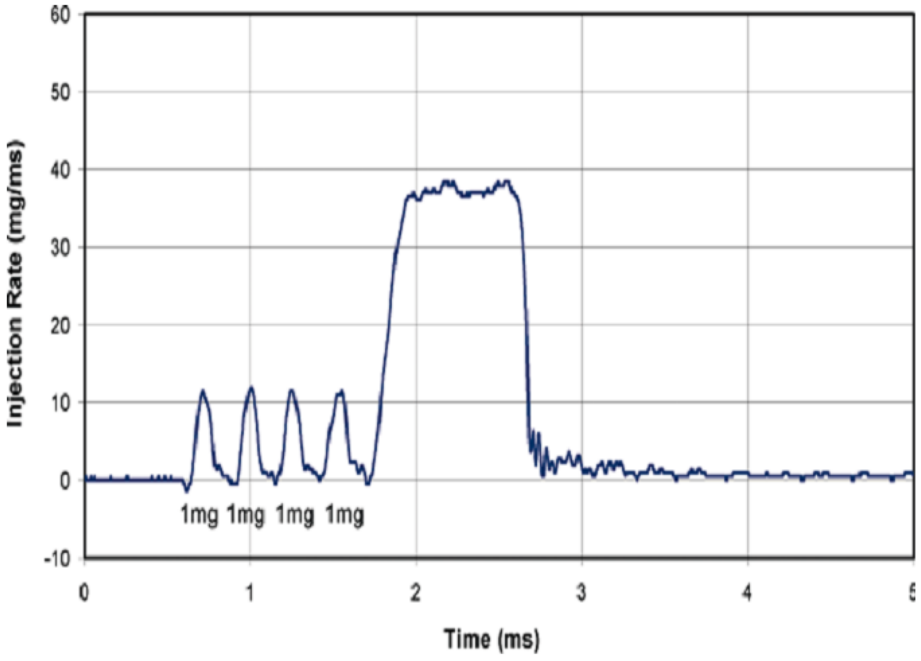

Figure 1.3: Injection rate over time during on combustion cycle from a multiple injection system is shown. Four pre-injections, each transporting $\sim 1\ mg$ diesel fuel followed by the main injection is shown.

Two or three dimensional transient models are connected with major consumption of time and costs. The benefit of transient simulations is not only to identify sources of error, but also to write an optimized software program for the control unit of the engine. Commercial available software tools for one dimensional modeling are often very expensive, and often have no suitable equation of state for liquid diesel fuel. The goal of this work was to try to create a simulation tool, which helps simulating the diesel fuel cycle in an engine by creating the basic components for a module construction of any type of closed fluid network. Therefore three components have been implemented as subroutines, that can be arranged in an arbitrary way. First the pipe is discussed, describing the inviscid pressure driven flow in pipes with circular cross section. Second, the volume describes storage volumes on the one hand, like the rail or the tank, but also pumps on the other hand. At last the throttle is the basis for describing valves and orifice plates.

The whole simulation tool was implemented in Matlab Simulink 2008b ©, because it uses a graphical interface and it makes the creation of complex simulation models very easy, by using the basic components. Also the software is widely spread amongst developers in the automotive industry. All calculations presented in the results were performed on an ordinary laptop with a Intel©Core Duo 2.19 GHz CPU and a working memory of 3 GB.

Chapter 2

Material and Methods

In this chapter we will provide the governing equations for

- the fluid flow of diesel fuel through a pipe of constant cross section,
- the flow of diesel fuel through a throttle,
- the compression of diesel fuel in a piston pump,
- the charge and discharge of diesel fuel in a storage volume.

Therefore the thermodynamic equations of state of diesel fuel and the Euler equations governing the flow are reviewed. Also numerical algorithms are discussed.

2.1 Equations of State for liquid diesel Fuel

Diesel fuel is a complex mixture consisting among others of hydrocarbons having different thermodynamic properties, i.e. boiling points, densities and so on [Mollenhauer, 2002]. The main constituent parts are paraffin, different naphtalenes and some aromatics. There are differences in compositions, depending on the origin of the fuel and also depending on the season of the year [Kolev, 2007].
Here, for simplicity liquid diesel fuel is assumed to be a pure substance. It is described by the thermal and caloric equation of state (*DEOS* - Diesel Equations Of State). The state of pure substances in one phase and in thermal equilibrium can be described by two independent variables. In the following the temperature T and the pressure p are chosen as independent state variables. Note that the *DEOS* have to satisfy the Maxwell relations[1] [Schneider and Haas, 2004]. We assume that the density $\rho = \rho(p, T)$ is a given function of pressure p and temperature T, which is known from measurements. The measured data is well represented by the following

[1] All Maxwell Relations can be found in text books on thermodynamics, for example [Schneider and Haas, 2004]

expression

$$\rho(p,T) = \sum_{i=1}^{3} \left(\sum_{j=1}^{3} A_{ij} \left(\frac{T}{T_{ref}} \right)^{j-1} \right) \left(\frac{p}{p_{ref}} \right)^{i-1} \rho_{ref} \tag{2.1}$$

with the pressure $p_{ref} = 1$ Pa, the temperature $T_{ref} = 1$ K and the density $\rho_{ref} = \rho(p_{ref}, T_{ref}) = 1$ kg/m^3 defining the system of units. The dimensionless coefficient matrix A is

$$A = \begin{pmatrix} 828.59744 & 0.63993 & -0.00216 \\ 8.65679\ 10^{-17} & -5.93672\ 10^{-9} & 1.56678\ 10^{-11} \\ -7.59052\ 10^{-16} & 8.99915\ 10^{-18} & -2.77890\ 10^{-20} \end{pmatrix},$$

as can be found in [Kolev, 2007]. A graph showing the density ρ as a function of pressure p and temperature T according to (2.1) is shown in Figure 2.1. To get the caloric equation of state, the isobaric heat capacity $c_p = c_p(p_0, T)$ at the constant reference pressure $p_0 = 1$ bar is needed. It has been taken from [Kolev, 2007]. Although in [Kolev, 2007] thermodynamic variables like speed of sound $c = c(p,T)$, the isobaric heat capacity $c_p = c_p(p,T)$ and many others are listed, they turn out to be inconsistent. For instance in equations (13.38) on page 285 and (13.43) on page 287 expressions for the heat capacity c_p and the derivative $\left(\frac{\partial h}{\partial p}\right)_T$ are given. However they do not satisfy the integrability condition

$$\frac{\partial}{\partial T}\left(\frac{\partial h}{\partial p}\right) = \frac{\partial}{\partial p}\left(\frac{\partial h}{\partial T}\right).$$

Evaluating both sides we obtain

$$-2.188\ 10^{-6} \frac{\mathrm{m}^3}{\mathrm{kgK}} \neq 0.456 \frac{\mathrm{m}^3}{\mathrm{kgK}}$$

for a pressure of $p = 1000$ bar and a temperature of $T = 313$ K.
Here we will derive an expression for the specific enthalpy h

$$h = h(p,T) \tag{2.2}$$

which is thermodynamically consistent, i.e. satisfies the Maxwell relations. We assume that the the density $\rho = \rho(p,T)$ as a function of pressure p and temperature T is given. Furthermore the heat capacity $c_p(T) = c_p(p_0, T)$ as functions of temperature T at a fixed reference pressure $p_0 = 1$ bar is given. If pressure p and temperature T are given as independent variables the Gibbs free energy $g = g(p,T)$ serves as a thermodynamic potential. With other words any thermodynamic variable can be expressed in terms of g or its derivatives. Starting with the Maxwell relation

$$\left(\frac{\partial g}{\partial p}\right)_T = \frac{1}{\rho(p,T)} \tag{2.3}$$

we obtain

$$g(p,T) = g_0(T) - g_0(T_0) + \int_{p_0}^{p} \frac{1}{\rho(p',T)} dp', \tag{2.4}$$

where $g_0(T)$ is an appropriate function, which has to be specified in the following. Writing the specific enthalpy h as a function of pressure p and specific entropy s

$$h(p,T) = h(p, s(p,T)) \tag{2.5}$$

we get the isobaric heat capacity

$$c_p(p,T) = \left(\frac{\partial h}{\partial T}\right)_p = \left(\frac{\partial h}{\partial s}\right)_p \left(\frac{\partial s}{\partial T}\right)_p. \tag{2.6}$$

Using the Maxwell relations $\left(\frac{\partial h}{\partial s}\right)_p = T$, $\left(\frac{\partial g}{\partial T}\right)_p = -s$ and (2.4) we can write for the isobaric heat capacity

$$c_p(p,T) = -T\frac{\partial^2 g(p,T)}{\partial T^2} = -T\left[g_0''(T) + \frac{\partial^2}{\partial T^2}\int_{p_0}^{p} \frac{1}{\rho(p',T)} dp'\right]. \tag{2.7}$$

Using the volumetric thermal expansion coefficient $\beta_p = -\frac{1}{\rho}\left(\frac{\partial \rho}{\partial T}\right)_p$, we obtain

$$c_p(p,T) = -Tg_0''(T) - T\left(\frac{\partial}{\partial T}\int_{p_0}^{p} \frac{1}{\rho(p',T)} \beta_p(p',T) \mathrm{d}p'\right)_p. \tag{2.8}$$

Inserting $p = p_0$ in equation (2.8) we get the auxiliary function g_0

$$g_0''(T) = -\frac{c_p(p_0,T)}{T}. \tag{2.9}$$

Therefore we have

$$c_p(p,T) = c_p(p_0,T) - T\left(\frac{\partial}{\partial T}\int_{p_0}^{p} \frac{1}{\rho(p',T)} \beta_p(p',T) \mathrm{d}p'\right)_p. \tag{2.10}$$

Now the isobaric heat capacity can be evaluated for any pressure and temperature. The specific enthalpy can be integrated from isobaric heat capacity

$$h(p,T) = \int_{T_0}^{T} c_p(p,T')dT' + h_0(p), \tag{2.11}$$

where $h_0(p) = h(p,T_0)$. Using (2.5) the chain rule for differentiation yields

$$\left(\frac{\partial h}{\partial p}\right)_T = \left(\frac{\partial h}{\partial p}\right)_s + \left(\frac{\partial h}{\partial s}\right)_p \left(\frac{\partial s}{\partial p}\right)_T = \frac{\partial}{\partial p}\left(\int_{T_0}^{T} c_p(p,T')dT' + h_0(p)\right) \tag{2.12}$$

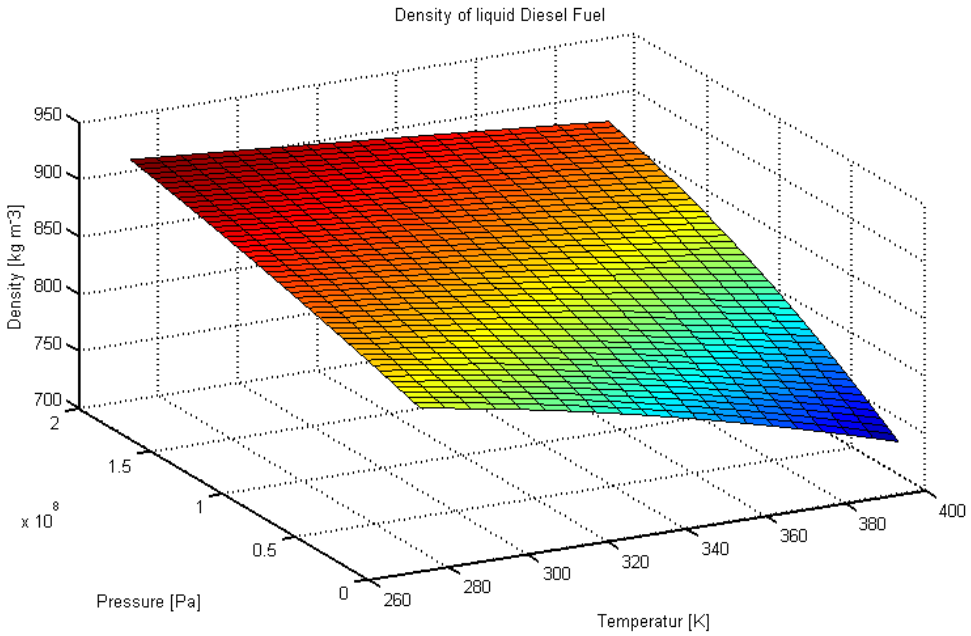

Figure 2.1: Density for liquid diesel fuel depending on temperature and pressure

and with the Maxwell relations $\left(\frac{\partial h}{\partial p}\right)_s = \frac{1}{\rho}$, $\left(\frac{\partial h}{\partial s}\right)_p = T$ and $\left(\frac{\partial s}{\partial p}\right)_T = \frac{1}{\rho^2}\left(\frac{\partial \rho}{\partial T}\right)_p$ we can write

$$\frac{1}{\rho} + \frac{T}{\rho^2}\left(\frac{\partial \rho}{\partial T}\right)_p = \frac{\partial}{\partial p}\int_{T_0}^{T} c_p(p, T')dT' + h_0'(p). \tag{2.13}$$

Evaluation of this expression at $T = T_0$ delivers an expression for the auxiliary function h_0

$$\frac{1}{\rho(p, T_0)}\left(1 - T_0\beta_p(p, T_0)\right) = h_0'(p). \tag{2.14}$$

Finally we obtain the specific enthalpy as

$$h(p, T) = h(p_0, T_0) + \int_{T_0}^{T} c_p(p, T')\,\mathrm{d}T' + \int_{p_0}^{p} \frac{1}{\rho(p', T)}\left(1 - T\,\beta_p(p', T)\right)\,\mathrm{d}p' \tag{2.15}$$

which is determined up to an arbitrary reference value for $h(p_0, T_0)$. Considering the range of temperature and pressure used in further applications, we chose specific enthalpy at a pressure of $p_0 = 1$ bar and a temperature of $T_0 = 253.15$ K, to vanish. The resulting numerical evaluations of this enthalpy function are shown in Figure 2.2.

The thermal and caloric equation of state, $\rho = \rho(p, T)$ and $h = h(p, T)$, and their derivatives with respect to both state variables, which will be evaluated numerically using predefined Matlab functions, are the basis for further considerations.

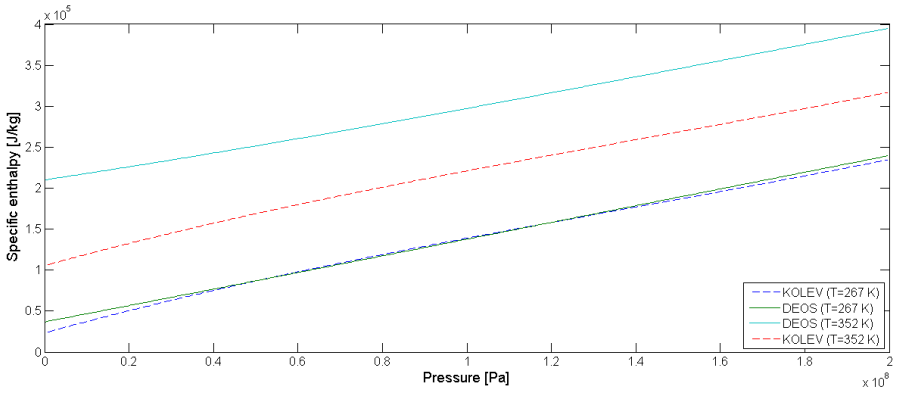

Figure 2.2: Specific enthalpy for liquid diesel fuel depending on pressure is shown. The enthalpy has been evaluated using (2.15) and using the approximation from [Kolev, 2007] for two different temperatures.

2.2 1-d Pipe Flow

The governing equations of fluid mechanics can be found in the literature, like for example [Landau and Lifshitz, 1987] or [Chorin and Marsden, 1993]. The flow in a pipe is influenced by transient phenomena, for example due to transient boundary conditions at both ends of the pipe and due to initial conditions in the pipe. Also the temperature of the fluid can change along the pipe depending on the outside temperature, the fluid temperature and the character of the cladding material of the pipe. Also changes in pressure lead to a change in temperature.

2.2.1 Governing equations

To calculate the one dimensional inviscid flow depending on time t and spatial coordinate x, three conservation laws have to be obeyed, which are: conservation of mass, momentum and energy. These conservation laws are valid for the whole pipe as well as for arbitrary small parts of the pipe. The conservation of mass can be written in the form:

$$\frac{\partial}{\partial t}\rho + \frac{\partial}{\partial x}(\rho u) = 0, \tag{2.16}$$

where u is the velocity and ρ the density of the fluid. The conservation of momentum can be written as

$$\frac{\partial}{\partial t}(\rho u) + \frac{\partial}{\partial x}(\rho u^2 + P) = 0, \tag{2.17}$$

where P is the pressure. Finally conservation law of total energy $E = E^i + E_{kin} = \rho(e + \frac{u^2}{2})$, consisting of internal energy $E^i = \rho e(P,T)$, with the specific internal energy $e = e(P,T)$, and kinetic energy $E_{kin} = \frac{\rho u^2}{2}$ is

$$\frac{\partial}{\partial t}E + \frac{\partial}{\partial x}((E + P)u) = 0. \tag{2.18}$$

These equations((2.16),(2.17),(2.18)) are known as the Euler equations. Here viscosity and heat conduction has been neglected [LeVeque, 2004]. Rewriting (2.16),(2.17),(2.18) in vector form

and using an abbreviation for the momentum $M = \rho u$, as well as using a vector of conserved state variables $\vec{q} = (\rho, M, E) \in \Omega \subset [\mathbf{R}^+, \mathbf{R}, \mathbf{R}]$, the general form of these conservation laws is

$$\vec{q}_t + f(\vec{q})_x = 0, \tag{2.19}$$

with the flux function $f(\vec{q}) : \mathbf{R}^p \to \mathbf{R}^p$ and subindices t and x indicating the differentiation with respect to time and space; More precisely

$$\frac{\partial}{\partial t}\begin{pmatrix}\rho\\ M\\ E\end{pmatrix} + \frac{\partial}{\partial x}\begin{pmatrix}M\\ \frac{M^2}{\rho}+P\\ \frac{(E+p)M}{\rho}\end{pmatrix} = 0. \tag{2.20}$$

The Jacobian $J = \frac{\partial f(\vec{q})}{\partial \vec{q}}$of the flux function $f(\vec{q})$ is

$$J = \begin{pmatrix} 0 & 1 & 0 \\ -\frac{M^2}{\rho^2} + \frac{\partial}{\partial \rho}P & 2\frac{M}{\rho} + \frac{\partial}{\partial M}P & \frac{\partial}{\partial E}P \\ \frac{M}{\rho}\left(-\frac{E+P}{\rho} + \frac{\partial}{\partial \rho}P\right) & \frac{E+P}{\rho} + \frac{M}{\rho}\frac{\partial}{\partial M}P & \frac{M}{\rho}\left(1 + \frac{\partial}{\partial E}P\right) \end{pmatrix}, \tag{2.21}$$

see [Guardone and Vigevano, 2001]. The Jacobian matrix J and its eigenvalues and eigenvectors are discussed in Appendix I.

2.2.2 Pressure Derivatives

In this section we want to determine the pressure derivatives of (2.21) in terms of thermodynamic quantities. In the Euler equations (2.20) we consider the pressure function

$$P = P(\rho, M, E) \tag{2.22}$$

as a function of conserved variables. Of course the pressure is also a function of the thermodynamic state variables internal energy per volume E^i and density ρ

$$p = p(E^i, \rho). \tag{2.23}$$

Since $E = E^i + \frac{\rho u^2}{2}$ we have

$$P(\rho, M, E) = p(E - \frac{M^2}{2\rho}, \rho). \tag{2.24}$$

Thus if we consider the pressure function as a function of the three conserved variables we use P with the capital letter, but if we consider the pressure function of the two thermodynamic variables we us p with the lower case letter. Derivatives of the pressure function follow to

$$\left(\frac{\partial P}{\partial \rho}\right)_{M,E} = \left(\frac{\partial p}{\partial \rho}\right)_{E^i} - \frac{1}{2}\frac{M^2}{\rho^2}\left(\frac{\partial p}{\partial E}\right)_{\rho}, \tag{2.25}$$

$$\left(\frac{\partial P}{\partial E}\right)_{\rho,M} = \left(\frac{\partial p}{\partial E^i}\right)_{\rho} \tag{2.26}$$

$$\left(\frac{\partial P}{\partial M}\right)_{\rho,E} = -\frac{M}{\rho}\left(\frac{\partial p}{\partial E^i}\right)_{rho}. \tag{2.27}$$

In order to determine the pressure derivatives $\left(\frac{\partial p}{\partial \rho}\right)_{E^i}$ and $\left(\frac{\partial p}{\partial E^i}\right)_{\rho}$ we need to change the independent variables $(p,T) \Longleftrightarrow (\rho, E^i)$. For the internal energy E^i and the density ρ we can write

$$E^i = \rho(p,T)h(p,T) - p, \tag{2.28}$$

$$\rho = \rho(p,T). \tag{2.29}$$

Considering the pressure $p = p(\rho, E^i)$ and the temperature $T = T(\rho, E^i)$ as functions of the density and the internal energy yields

$$E^i = \rho(p(\rho,E^i),T(\rho,E^i))h(p(\rho,E^i),T(\rho,E^i)) - p, \tag{2.30}$$

$$\rho = \rho(p(\rho,E^i),T(\rho,E^i)). \tag{2.31}$$

Differentiating the expressions (2.30), (2.31) with respect to internal energy E^i follows

$$1 = h\left[\left(\frac{\partial \rho}{\partial p}\right)_T\left(\frac{\partial p}{\partial E^i}\right)_{\rho} + \left(\frac{\partial \rho}{\partial T}\right)_p\left(\frac{\partial T}{\partial E^i}\right)_{\rho}\right] + \rho\left[\left(\frac{\partial h}{\partial p}\right)_T\left(\frac{\partial p}{\partial E^i}\right)_{\rho} + \left(\frac{\partial h}{\partial T}\right)_p\left(\frac{\partial T}{\partial E^i}\right)_{\rho}\right] - \left(\frac{\partial p}{\partial E^i}\right)_{\rho}$$

$$0 = \left(\frac{\partial \rho}{\partial p}\right)_T\left(\frac{\partial p}{\partial E^i}\right)_{\rho} + \left(\frac{\partial \rho}{\partial T}\right)_p\left(\frac{\partial T}{\partial E^i}\right)_{\rho}$$

As a result an expression for the pressure derivative with respect to internal energy E^i, that depends only on known quantities from the equations of state, can be formulated

$$\left(\frac{\partial p}{\partial E^i}\right)_{\rho} = \left[\rho\left(\left(\frac{\partial h}{\partial p}\right)_T - \frac{\left(\frac{\partial h}{\partial T}\right)_p\left(\frac{\partial \rho}{\partial p}\right)_T}{\left(\frac{\partial \rho}{\partial T}\right)_p}\right) - 1\right]^{-1}. \tag{2.32}$$

Analogously we can differentiate (2.30), (2.31) with respect to density ρ

$$0 = h\left[\left(\frac{\partial \rho}{\partial p}\right)_T\left(\frac{\partial p}{\partial \rho}\right)_{E^i} + \left(\frac{\partial \rho}{\partial T}\right)_p\left(\frac{\partial T}{\partial \rho}\right)_{E^i}\right] + \rho\left[\left(\frac{\partial h}{\partial p}\right)_T\left(\frac{\partial p}{\partial \rho}\right)_{E^i} + \left(\frac{\partial h}{\partial T}\right)_p\left(\frac{\partial T}{\partial \rho}\right)_{E^i}\right] - \left(\frac{\partial p}{\partial \rho}\right)_{E^i},$$

$$1 = \left(\frac{\partial \rho}{\partial p}\right)_T\left(\frac{\partial p}{\partial \rho}\right)_{E^i} + \left(\frac{\partial \rho}{\partial T}\right)_p\left(\frac{\partial T}{\partial \rho}\right)_{E^i}.$$

Now an expression for the pressure derivative with respect to density ρ, again depending only on known quantities from *DEOS* , can be formulated to

$$\left(\frac{\partial p}{\partial \rho}\right)_{E^i} = \frac{-h - \rho\frac{\left(\frac{\partial h}{\partial T}\right)_p}{\left(\frac{\partial \rho}{\partial T}\right)_p}}{\rho\left(\frac{\partial h}{\partial p}\right)_T - \rho\frac{\left(\frac{\partial \rho}{\partial p}\right)_T\left(\frac{\partial h}{\partial T}\right)_p}{\left(\frac{\partial \rho}{\partial T}\right)_p} - 1}. \tag{2.33}$$

In terms of common thermodynamic properties using the definition of the isothermal compressibility $\chi = \frac{1}{\rho}\left(\frac{\partial \rho}{\partial p}\right)_T$, the isobaric heat capacity $c_p = \left(\frac{\partial h}{\partial T}\right)_p$, the isobaric coefficient of expansion $\beta = -\frac{1}{\rho}\left(\frac{\partial \rho}{\partial T}\right)_p$, and using the relation $\left(\frac{\partial h}{\partial p}\right)_T = \frac{1-T\beta}{\rho}$ (see [Schneider and Haas, 2004]), we can rewrite the equations (2.32) and (2.33)

$$\left(\frac{\partial p}{\partial E^i}\right)_\rho = \frac{\beta}{T\beta^2 + \rho c_p \chi}, \tag{2.34}$$

$$\left(\frac{\partial p}{\partial \rho}\right)_{E^i} = \frac{h - \frac{c_p}{\beta}}{T\beta - \frac{\rho c_p \chi}{\beta}}. \tag{2.35}$$

Thus we have

$$\left(\frac{\partial P}{\partial \rho}\right)_{M,E} = \frac{\beta h - c_p}{T\beta^2 - \rho c_p \chi} - \frac{M^2}{2\rho^2}\frac{\beta}{T\beta^2 + \rho c_p \chi}, \tag{2.36}$$

$$\left(\frac{\partial P}{\partial E}\right)_{\rho,M} = \frac{\beta}{T\beta^2 + \rho c_p \chi}, \tag{2.37}$$

$$\left(\frac{\partial P}{\partial M}\right)_{\rho,E} = -\frac{M}{\rho}\frac{\beta}{T\beta^2 + \rho c_p \chi} \tag{2.38}$$

2.2.3 Numerical Methods

One-dimensional Finite Volume Method

The following concepts for solving conservation laws in one spatial direction are covered in the literature, see for example [LeVeque, 2004] or [Toro, 2009].
The finite volume method is based on dividing the region of interest into intervals (the "finite volumes" or so called "grid cells", or "cells") and is also based on approximating the integral of the state vector $\mathbf{q} = \vec{q}$ over each of those cells. The intervals $\mathcal{C}_i$ have a constant length Δx, a midpoint x_i and can be denoted by

$$\mathcal{C}_i = (x_{i-\frac{1}{2}}, x_{i+\frac{1}{2}}) \tag{2.39}$$

where the cell boundary on the left side is located at $x_{i-\frac{1}{2}} = \frac{1}{2}(x_i + x_{i-1})$ and on the right side at $x_{i+\frac{1}{2}} = \frac{1}{2}(x_i + x_{i+1})$, as shown in Figure 2.3. The value Q_i^n approximates the average value

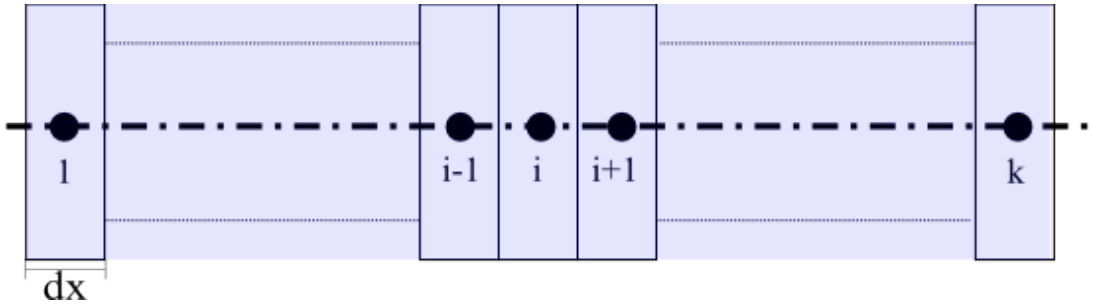

Figure 2.3: Subdivision of a pipe (blue) into k Cells with length dx and midpoint $x_i = 1...k$ (black dots).

of the state vector over the ith interval at time t_n:

$$Q_i^n \approx \frac{1}{\Delta x} \int_{x_{i-\frac{1}{2}}}^{x_{i+\frac{1}{2}}} \mathbf{q}(x, t_n)\, dx \equiv \frac{1}{\Delta x} \int_{\mathcal{C}_i} \mathbf{q}(x, t_n)\, dx. \tag{2.40}$$

Note that only uniform grids and pipes with no change in cross-section will be discussed here. Integrating the differential form of the quasi one-dimensional Euler equation

$$\frac{\partial}{\partial t}\mathbf{q} + \frac{\partial}{\partial x}\mathbf{f}(\mathbf{q}) = 0 \tag{2.41}$$

over the cell $\mathcal{C}_i$ and one time interval $[x_{i-\frac{1}{2}}, x_{i+\frac{1}{2}}] \times [t_n, t_{n+1}]$ yields the integral formulation:

$$\int_{x_{i-\frac{1}{2}}}^{x_{i+\frac{1}{2}}} \mathbf{q}(x, t_{n+1})\, dx - \int_{x_{i-\frac{1}{2}}}^{x_{i+\frac{1}{2}}} \mathbf{q}(x, t_n)\, dx + \int_{t_n}^{t_{n+1}} \mathbf{f}(\mathbf{q}(x_{i+\frac{1}{2}}, t)\, dt - \int_{t_n}^{t_{n+1}} \mathbf{f}(\mathbf{q}(x_{i-\frac{1}{2}}, t)\, dt = 0. \tag{2.42}$$

The state vector $\mathbf{q}$ and the analytical flux function $\mathbf{f}$ depend on spatial coordinate x and time t. The first two terms in (2.42) represent the total fluxes of the state quantities across the boundaries $x_{i+\frac{1}{2}}$ and $x_{i-\frac{1}{2}}$. The third and fourth terms correspond to the total change of state quantities inside cell $\mathcal{C}_i$ during the time step $\Delta t = tn+1-tn$. Therefore the system of equations (2.42) states, that every gain or loss of state quantities inside the cell is due to the fluxes across the boundaries. Implicitly the conservation of the state quantities within the whole region of interest will be ensured. However in general we cannot evaluate the time integrals exactly, since $\mathbf{q}(x_{i\pm\frac{1}{2}}, t)$ varies with time along each edge of the cell, and we dont have the exact solution to work with. To cope with this problem we use a numerical method of the form

$$Q_i^{n+1} = Q_i^n - \frac{\Delta t}{\Delta x}(F_{i+\frac{1}{2}}^n - F_{i-\frac{1}{2}}^n) \tag{2.43}$$

where $F_{i\pm\frac{1}{2}}$ is some approximation to the average flux along the left and the right boundary of the i-th cell respectively,

$$F_{i-\frac{1}{2}}^n \approx \frac{1}{\Delta t} \int_{t_n}^{t_{n+1}} \mathbf{f}(\mathbf{q}(x_{i-\frac{1}{2}}, t)\, dt. \tag{2.44}$$

Rearranging (2.43) we can express the change in state for each cell as

$$\frac{d\,Q_i}{dt} = \frac{Q_i^{n+1} - Q_i^n}{\Delta t} = \frac{F^n_{i+\frac{1}{2}} - F^n_{i-\frac{1}{2}}}{\Delta x} \tag{2.45}$$

where the left hand side represents the change in time, which has been calculated using ordinary differential equation solvers (ODE solvers) predefined in Matlab. These solvers can be found in the Matlab manual or in [Shampine and Reichelt, 1997]. The right hand side has been numerically evaluated using an approximation for the flux function $F_{i\pm\frac{1}{2}}$.

Roe's Linearization

This method is well documented in the literature (see, e.g., [LeVeque, 2004]) and will only be briefly outlined here.
The Roe approximate Riemann solver has been introduced by Phil Roe and is a Gudonov type scheme based on a local linearization of the considered hyperbolic system of conservation laws [Roe, 1981]. This method makes no assumption on the equation of state, and, in this respect, is more flexible than the flux split methods [Guardone and Vigevano, 2001]. At every cell boundary $x_{i-\frac{1}{2}}$ the associated Riemann problem is replaced by a linear Riemann problem

$$\frac{\partial}{\partial t}\mathbf{q} + \hat{A}^n_{i-\frac{1}{2}}\frac{\partial}{\partial x}\mathbf{q} = 0 \tag{2.46}$$

where the so called Roe-matrix $\hat{A}^n_{i-\frac{1}{2}}$ is chosen to be an approximation to $\mathbf{f}'(\mathbf{q})$ valid in a neighborhood of the data Q_{i-1} and Q_i. Further the Roe-matrix has to satisfy following conditions:

- Conservation: $\hat{A}^n_{i-\frac{1}{2}}(\mathbf{q}_i^n - \mathbf{q}_{i-1}^n) = \mathbf{f}(\mathbf{q}_i^n) - \mathbf{f}(\mathbf{q}_{i-1}^n)$
- Hyperbolicity: $\hat{A}^n_{i-\frac{1}{2}}$ has real eigenvalues $\hat{\lambda}^p_{i-\frac{1}{2}}$ and a corresponding set of eigenvectors $\hat{r}^p_{i-\frac{1}{2}}$ that form a basis of $\mathbf{R}^p$
- Consistency: $\hat{A}^n_{i-\frac{1}{2}}(\mathbf{q}_{i-1}^n, \mathbf{q}_i^n) \rightarrow J(\mathbf{q}) = \frac{\partial \mathbf{f}(\mathbf{q})}{\partial \mathbf{q}}$ when $\mathbf{q}_i^n$ and $\mathbf{q}_{i-1}^n \rightarrow \mathbf{q}$

with $p = 3$ for the Euler equations in one spatial dimension. The approximate Riemann solution then consists of waves $\mathcal{W}^p$ proportional to the eigenvectors $\hat{r}^p_{i-\frac{1}{2}}$ of $\hat{A}_{i-\frac{1}{2}}$, propagating with speeds $s^p_{i-\frac{1}{2}} = \hat{\lambda}^p_{i-\frac{1}{2}}$ given by the eigenvalues. The waves can be obtained by solving the linear system

$$Q_i - Q_{i-1} = \sum_{p=1}^{3} \alpha^p_{i-\frac{1}{2}}\hat{r}^p_{i-\frac{1}{2}} \tag{2.47}$$

for the coefficients $\alpha^p_{i-\frac{1}{2}}$ and then setting $\mathcal{W}^p_{i-\frac{1}{2}} = \alpha^p_{i-\frac{1}{2}} \hat{r}^p_{i-\frac{1}{2}}$.
To get the Roe-matrix, the conservation condition can be rewritten

$$\begin{pmatrix} 0 & 1 & 0 \\ -\frac{\hat{M}^2}{\hat{\rho}^2} + \frac{\partial}{\partial\hat{\rho}}\hat{P} & 2\frac{\hat{M}}{\hat{\rho}} + \frac{\partial}{\partial\hat{M}}\hat{P} & \frac{\partial}{\partial\hat{E}}\hat{P} \\ \frac{\hat{M}}{\hat{\rho}}\left(-\frac{\hat{E}+\hat{P}}{\hat{\rho}} + \frac{\partial}{\partial\hat{\rho}}\hat{P}\right) & \frac{\hat{E}+\hat{P}}{\hat{\rho}} + \frac{\hat{M}}{\rho}\frac{\partial}{\partial\hat{M}}\hat{P} & \frac{\hat{M}}{\hat{\rho}}\left(1 + \frac{\partial}{\partial\hat{E}}\hat{P}\right) \end{pmatrix} \begin{pmatrix} \rho_i - \rho_{i-1} \\ M_i - M_{i-1} \\ E_i - E_{i-1} \end{pmatrix} = \begin{pmatrix} M_i - M_{i-1} \\ \frac{M_i^2}{\rho_i} + P_i - \frac{M_{i-1}^2}{\rho_{i-1}} - P_{i-1} \\ \frac{(E_i+P_i)M_i}{\rho_i} - \frac{(E_{i-1}+P_{i-1})M_{i-1}}{\rho_{i-1}} \end{pmatrix} \tag{2.48}$$

where expressions with ' $\hat{.}$ ' denote Roe averaged quantities. Obviously the equation in the first line of (2.48) is trivial, since no Roe averaged states appear in this equation. The derivatives of the pressure function, which are derived in chapter 2.2.2, are now functions of Roe averaged state variables $\hat{p}$ and $\hat{T}$ as well as the density $\hat{\rho} = \rho(\hat{p}, \hat{T})$ known from *DEOS*. Following Roe we set the averaged velocity $\hat{u} = \frac{\hat{M}}{\hat{\rho}}$ and the averaged total enthalpy $\hat{H} = \frac{\hat{E}+\hat{p}}{\hat{\rho}}$

$$\frac{\hat{M}}{\hat{\rho}} = \frac{\frac{M_{i-1}}{\sqrt{\rho_{i-1}}} + \frac{M_i}{\sqrt{\rho_i}}}{\sqrt{\rho_{i-1}} + \sqrt{\rho_i}} \tag{2.49}$$

and

$$\hat{H} = \frac{\sqrt{\rho_{i-1}}H_{i-1} + \sqrt{\rho_i}H_i}{\sqrt{\rho_{i-1}} + \sqrt{\rho_i}} = \frac{\frac{E_{i-1}+p_{i-1}}{\rho_{i-1}} + \frac{E_i+p_i}{\rho_i}}{\sqrt{\rho_{i-1}} + \sqrt{\rho_i}}. \tag{2.50}$$

It remains to determine $\hat{\rho}$, and thus $\hat{p}$ and $\hat{T}$. It turns out that the second and third equation in (2.48) are satisfied if

$$\frac{\partial\hat{P}}{\partial\hat{\rho}}(\rho_i - \rho_{i-1}) + \frac{\partial\hat{P}}{\partial\hat{M}}(M_i - M_{i-1}) + \frac{\partial\hat{P}}{\partial\hat{E}}(E_i - E_{i-1}) = p_i - p_{i-1} \tag{2.51}$$

holds, see [Guardone and Vigevano, 2001]. Inserting the expressions for the pressure derivatives (2.25), (2.26), (2.27) and equation (2.49) for the averaged velocity turns the supplementary equation into

$$\frac{\partial\hat{p}}{\partial\hat{\rho}}(\rho_i - \rho_{i-1}) + \frac{\partial\hat{p}}{\partial\hat{E}^i}(E^i_i - E^i_{i-1}) = p_i - p_{i-1}, \tag{2.52}$$

where E^i denotes the internal energy. The exact derivation of this equation can be found here [Guardone and Vigevano, 2001]. If now one inserts the expressions (2.35) and (2.34) for the pressure derivatives, the supplementary equation is depending on two averaged state quantities $\hat{p}$ and $\hat{T}$. These quantities define the Roe matrix for any pair of states Q_{i-1} and Q_i. To find a Roe Matrix, a second conditional equation is needed, what for the caloric equation of state is used in the conditional form

$$h(\hat{p}, \hat{T}) = \hat{H} - \frac{1}{2}\left(\frac{\hat{M}}{\hat{\rho}}\right)^2 \tag{2.53}$$

Those two equations ((2.52),(2.53)) determine the averaged pressure $\hat{p}$ and the averaged temperature $\hat{T}$ and thus the Roe matrix. To solve these equations, in order to get values of $\hat{p}$ and $\hat{T}$, a Levenberg-Marquardt algorithm has been used, which is a preimplemented function in Matlab, that is described in the Matlab manual or in [Levenberg, 1944]. After the Roe matrix is found, numerical evaluation of the associated eigenvalues $\hat{\lambda}^p$, eigenvectors $\hat{r}^p$, that are building up the eigenbasis $R_{i-\frac{1}{2}}$, can be done and the numerical flux function

$$F^n_{i-\frac{1}{2}} = \frac{1}{2}(\mathbf{f}(Q_{i-1}) + \mathbf{f}(Q_i)) + \frac{1}{2}\sum_{p=1}^{3} \left|\hat{\lambda}^p_{i-1/2}\right| \mathcal{W}^p_{i-1/2} \tag{2.54}$$

can be evaluated. Note that this numerical flux function can be found in [LeVeque, 2004].

2.2.4 Source Terms

In order to take into account that heat can be transfered into and out of the fluid trough the surface of the pipe, the governing equations have to be changed into

$$\vec{q}_t + f(\vec{q})_x = \mathbf{\Psi}, \tag{2.55}$$

with the source term vector $\mathbf{\Psi}$. This model of the pipe has no friction term included and also heat transfer within the fluid is neglected. Only heat transfered through the surface of the pipe is taken into account. Therefore the source term vector is defined by

$$\Psi = \begin{pmatrix} 0 \\ 0 \\ \frac{\lambda_h}{d} A_s (T_{ext} - T) \end{pmatrix}, \tag{2.56}$$

where d denotes the wall thickness of the pipe, λ_h describes the thermal conductivity of the pipe material, A_s is the surface of one finite volume and T_{ext} is the temperature outside the pipe. The time evolution of the approximate state vector Q^{n+1}_i with source terms is

$$\frac{dQ_i}{dt} = \frac{Q^{n+1}_i - Q^n_i}{\Delta t} = \frac{F^n_{i+\frac{1}{2}} - F^n_{i-\frac{1}{2}}}{\Delta x} + \Psi. \tag{2.57}$$

2.3 Volume

Here the conservation laws for mass and energy shall be discussed for an open thermodynamic system like a fluid reservoir, where kinetic energies can be neglected. As boundary conditions mass flow, into and out of the reservoir, and a change in size of the reservoir, which is the case in pumps for example, are given. The volume shall calculate the inner parameters of the fluid such as compressibility, enthaply, density and other fluid parameters resulting out of *DEOS* . Therefore the time evolutions of pressure and temperature are searched.
Starting with the conservation of mass, the change in mass in the vessel equals an external mass

flow, which is assumed to be a transient boundary condition

$$\frac{dm}{dt} = \dot{m}_{ext} = \sum_i \dot{m}^i_{ext}, \tag{2.58}$$

where i denotes the number of components that are connected to this vessel. Introducing the specific volume $v = \frac{1}{\rho}$ the total mass $m = \rho V = \frac{V}{v}$ is a function of specific volume and total volume, and then (2.58) can be rewrite as

$$\frac{dm}{dt} = \frac{1}{v}\left(\frac{dV}{dt}\right)_{ext} - \frac{V}{v^2}\frac{dv}{dt} = \dot{m}_{ext}, \tag{2.59}$$

where quantities with the subindex $_{ext}$ denote boundary conditions. Now an equation for the change in density can be formulated out of the conservation of mass

$$-\frac{1}{\rho^2}\frac{d\rho}{dt} = \frac{dv}{dt} = \frac{1}{V}\left[v\left(\frac{dV}{dt}\right)_{ext} - v^2\dot{m}_{ext}\right] \tag{2.60}$$

The conservation of energy is expressed by the first law of thermodynamics

$$\frac{dE}{dt} = \dot{W} + \dot{Q} + \sum_i \dot{m}^i_{ext} h^i_{ext} \tag{2.61}$$

where E is the total energy, $\dot{W}$ the work done on the system, $\dot{Q}$ heat added to the system and $\sum_i \dot{m}^i_{ext} h^i_{ext}$ the sum of all enthalpy currents into or out of the system. Since in the vessel kinetic energies are neglected, total energy equals the internal energy $E = E^i(v, T)$. Due to simplicity it is assumed that work done on the system only refers to compression work

$$\dot{W} = -p\frac{dV}{dt}. \tag{2.62}$$

Heat transfered through the boundary into the volume can be described through a linear, one dimensional heat transfer. The volume is bounded by a wall with the surface area A and with a wall thickness b and the thermal conductivity λ, so the heat transfered is proportional to the temperature gradient between outside(T_o) and inside(T_i) the volume

$$\dot{Q} = \frac{A\lambda}{b}(T_o - T_i). \tag{2.63}$$

Note that in reciprocating compressors convective heat transfer may play an important role. Since stationary vortices can cause high velocities inside the compressor more heat is transfered over the surface (T. Müllner 2010, pers. comm.). Therefore in this model the thermal conductivity λ is an effective heat transfer coefficient, which can have higher values than the actual thermal conductivity then for the supposed cladding material. Introducing the specific inner

energy $e(v,T) = \frac{E^i(v,T)}{m}$ equation (2.61) can be rewritten as

$$\frac{dE}{dt} = \frac{dE^i}{dt} = \frac{dm}{dt}e + m\frac{de}{dt} \tag{2.64}$$

Inserting equation (2.58) and decomposing the differential of the specific internal energy e it follows

$$(\sum_i \dot{m}^i_{ext})e + m\left[\left(\frac{\partial e}{\partial T}\right)_v \frac{dT}{dt} + \left(\frac{\partial e}{\partial v}\right)_T \frac{dv}{dt}\right] = -p\frac{dV}{dt} + \frac{A\lambda}{b}(T_o - T) + \sum_i \dot{m}^i_{ext}h^i_{ext} \tag{2.65}$$

From Gibbs fundamental equation

$$ds = \frac{1}{T}\left(\frac{\partial e}{\partial T}\right)_v dT + \frac{1}{T}\left[\left(\frac{\partial e}{\partial v}\right)_T + p\right]dv, \tag{2.66}$$

the expression for the partial derivative of the specific internal energy e with respect to the specific volume v

$$\left(\frac{\partial e}{\partial v}\right)_T = (T\left(\frac{\partial s}{\partial v}\right)_T - p) \tag{2.67}$$

can be developed for constant temperatures. The expression in the bracket in equation (2.65) can then be simplified into

$$\left(\frac{\partial e}{\partial T}\right)_v \frac{dT}{dt} + \left(\frac{\partial e}{\partial v}\right)_T \frac{dv}{dt} = c_v\frac{dT}{dt} + (T\left(\frac{\partial s}{\partial v}\right)_T - p)\frac{dv}{dt} \tag{2.68}$$

where $c_v = \left(\frac{\partial e}{\partial T}\right)_v$ describes the isochoric heat capacity. Using the Maxwell relation $\left(\frac{\partial s}{\partial v}\right)_T = \left(\frac{\partial p}{\partial T}\right)_v$ we can solve for transient temperature change

$$\frac{dT}{dt} = -\frac{1}{c_v}\left[(T\left(\frac{\partial p}{\partial T}\right)_v - p)\frac{dv}{dt} + \frac{1}{m}\left(p\frac{dV}{dt} - \frac{A\lambda}{b}(T_o - T) - (\sum_i \dot{m}^i_{ext}h^i_{ext}) + (\sum_i \dot{m}^i_{ext})e\right)\right] \tag{2.69}$$

which only depends on quantities known from *DEOS* , because of $\left(\frac{\partial p}{\partial T}\right)_v = \frac{\beta_p}{\chi_T}$ and $c_v = c_p - \frac{T\beta_p^2}{\chi_T\rho}$ (see [Schneider and Haas, 2004]). Both, time evolution of the density and time evolution of the temperature, are then evaluated using the Matlab ODE solvers [Shampine and Reichelt, 1997].

2.4 Throttle

Here the influence of a thin orifice plate on the fluid flow is discussed. We will calculate the mass flow depending on the pressure difference between both sides of the throttle, and also calculate the change in temperature of the fluid after passing the throttle. The key parameter for this device is a ratio of the diameters between the diameter of the obstruction D_2,where the flow is

forced through, and the diameter of the inlet and discharge pipe D as can be seen in Figure 2.4

$$\gamma = \frac{D_2}{D}. \tag{2.70}$$

After the flow passed the obstruction, the actual cross section, that conveys mass, is contracted to the diameter $D_2 < d$ [White, 2006], see Figure 2.4. Starting with the mass balance

$$\frac{D^2\pi}{4} u_1 \rho = \frac{D_2^2\pi}{4} u_2 \rho, \tag{2.71}$$

where u_1 and u_2 are an averaged velocity before and after the obstruction.Using Bernoulli's law

$$p_1 + \frac{\rho u_1^2}{2} = p_2 + \frac{\rho u_2^2}{2}, \tag{2.72}$$

the mass flow can be calculated to

$$\dot{m} = \frac{D_2^2\pi}{4} \sqrt{\frac{2\rho(p_1 - p_2)}{(1 - \frac{D_2^4}{D^4})}} \tag{2.73}$$

Note that all considerations in this section assume an incompressible fluid without friction, which is not accurate for real applications. Therefore equation (2.73) has to be modified. Also equation (2.73) can only deliver results for $p_1 > p_2$, because of the root function, what has to be changed in order to function omnidirectional. Using the sign function sgn and introducing the friction coefficient C_d, the mass flow equation (2.73) can be changed into

$$\dot{m} = sgn(p_1 - p_2) \frac{d^2\pi}{4} C_d \sqrt{\frac{2\rho(|p_1 - p_2|)}{(1 - \gamma^4)}} \tag{2.74}$$

Note that due to simplify the model, the diameter of the obstruction d and the diameter of the contracted vein are assumed to be equal $d = D_2$. The friction coefficient $C_d = C_d(\gamma, Re)$ depends on the diameter ratio as well as on the Reynolds number ($Re = \frac{u_1 D}{\nu}$), with kinematic viscosity ν). The following curve fit for approximating the friction coefficient for thin orifice plates is used

$$C_d(\gamma, Re) = 0.5959 + 0.0312\gamma^{2.1} - 0.184\gamma^8 + 91.71\gamma^{2.5} Re^{-0.75}, \tag{2.75}$$

which can be found in [White, 2006].
Now also the change in temperature shall get determined by the pressure difference $\Delta p = p_1 - p_2$. We assume that the specific enthaply does not change while the fulid passes through the throttle. This assumption is valid if heat exchange with the surroundings is neglected, the kinetic energy of the fluid does not change and no work is done on the fluid. Starting with Gibbs fundamental equation

$$dh = Tds + vdp = 0 \tag{2.76}$$

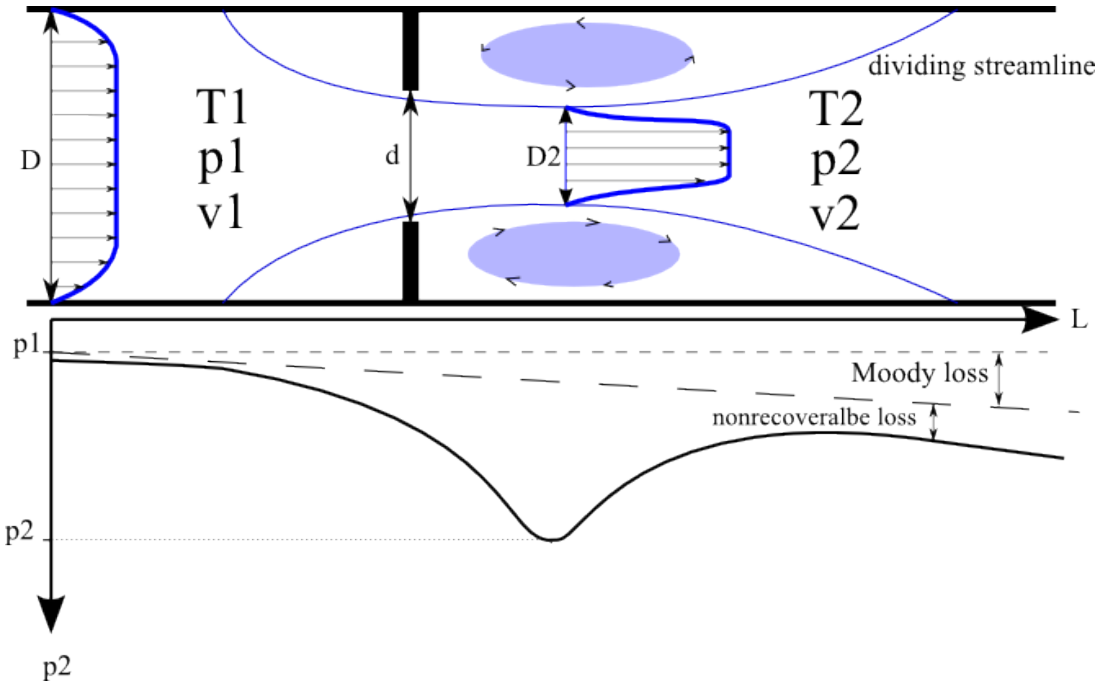

Figure 2.4: Schematic velocity and schematic pressure change trough a generalized Bernoulli obstruction meter

the entropy differential can be reformulated due to the assumption $s = s(p, T)$, so that

$$0 = T\left(\frac{\partial s}{\partial T}\right)_p dT + \left[v + T\left(\frac{\partial s}{\partial p}\right)_T\right] dp. \tag{2.77}$$

Inserting the definition of the specific heat capacity $c_p = T\left(\frac{\partial s}{\partial T}\right)_p = \left(\frac{\partial h}{\partial T}\right)_p$ follows

$$0 = c_p dT + \left[v + T\left(\frac{\partial s}{\partial p}\right)_T\right] dp. \tag{2.78}$$

Now using the Maxwell Relation $\left(\frac{\partial s}{\partial p}\right)_T = -\left(\frac{\partial v}{\partial T}\right)_p$ and introducing the linear expansion coefficient $\beta_p = \frac{1}{v}\left(\frac{\partial v}{\partial T}\right)_p$ yields

$$\left(\frac{\partial T}{\partial p}\right)_h = \frac{v(T\beta_p - 1)}{c_p}, \tag{2.79}$$

an expression for the Joule-Thomson coefficient $\left(\frac{\partial T}{\partial p}\right)_h$, depending on *DEOS*. The Joule-Thompson coefficient can have a negative or positive sign, or equals zero for an ideal gas. For diesel however it turns out that the Joule-Thompson coefficient is negative. Thus during throttling of diesel the temperature increases. For solving the temperature progression the equation (2.78) can be reformulated

$$(T\beta_p - 1)^{-1} dT = \frac{v}{c_p} dp. \tag{2.80}$$

Introducing the auxiliary function $\chi = T\beta_p - 1$ and inserting the differential $\beta_p^{-1} d\chi = dT$ this can be transformed into

$$\frac{1}{\beta_p}\frac{d\chi}{\chi} = \frac{v}{c_p}dp, \tag{2.81}$$

and after integrating both sides

$$\chi_2 = \exp\left(\frac{v\beta_p}{c_p}(p_2 - p_1)\right)\chi_1 \tag{2.82}$$

and reinserting the expression for χ, follows the solution for the temperature of the fluid after it passed the throttle T_2:

$$T_2 = \frac{\exp\left(\frac{v\beta_p}{c_p}(p_2 - p_1)\right)(T_1\beta_p - 1) + 1}{\beta_p}, \tag{2.83}$$

where T_1 is the temperature of the fluid at the intake of the throttle.

2.5 Boundary conditions

In order to create a physical model of a hydrodynamic network containing pipes, volumes and throttles, the single components have to exchange information. This section is on the informations the single components need as input for setting boundary conditions, and also on the informations the single components give back to other components.
The pipe simulates the flow in a straight pipe without cross section changes. Therefore it can be connected to two other components, one at the left and one at the right end of the pipe. Two different versions of the pipe have been implemented. One implementation only needs the pressure and temperature from both connected components, because the momentum is assumed to have a vanishing gradient using ghost cells [LeVeque, 2004]. This implementation is for connecting the pipe with volumes. On each side of the pipe it is analyzed if the fluid is flowing into the pipe or out of the pipe. As an outflow boundary condition the pressure in the cell next to the volume is set to the same value as prevailing in the connected volume. As an inflow boundary condition the pressure and the temperature in the cell next to the volume has to satisfy the following conditions. Due to the conservation of energy the first condition can be written as

$$h(p_c, T_c) + \frac{u^2}{2} = h(p_V, T_V), \tag{2.84}$$

with pressure and temperature in the cell indicated by subindex $_c$, in the connected volume by subindex $_V$ and with the velocity u in the cell. Since no friction or heat transfer is taken into account the inflow is assumed to be isentropic ($ds = 0$). According to Gibbs fundamental equation

$$ds = \frac{c_p}{T}dT - \left(\frac{\partial v}{\partial T}\right)_p dp, \tag{2.85}$$

see [Schneider and Haas, 2004], the second condition can be rewritten as

$$\int_{T_V}^{T_c} c_p(p, T')dT' + \int_{pV}^{p_c} T\frac{\beta(p', T)}{\rho(p', T)}dp' = 0. \tag{2.86}$$

The other implementation of the pipe needs the pressure, the temperature and the mass flow at both ends. Here these informations determine the state vector at the left and right end of the pipe completely. The outside temperature, the wall thickness and the heat conductivity of the pipe material also have to be set. In order to provide boundary conditions for the connected components the informations on pressure, temperature and mass flow are given back from next to the first and next to the last cell of the pipe.
The throttle needs the information on pressure from both connected components, from which it calculates the mass flow and the temperature change in the flow. Therefore it also needs the temperature from the incoming flow, which will be indicated by subindex $_l$, assuming that the fluid is flowing from the left side to the right side. The throttle gives back the information on mass flow at both sides and temperature on the right side (in flow direction).
The volume can connect to any number of surrounding components. The volume needs information on mass flows and enthalpy flows $\dot{h} = \dot{m}h(p, T)$ from every connected component and returns information on pressure and temperature inside the volume. Also the change in volume with time $\frac{d\ V_{ext}}{dt} = \frac{\partial V}{\partial t}$ is needed as a boundary condition.
The following table gives an overview over the committed quantities.

Components	Input	Output
Pipe	$p_{l,r}$, $T_{l,r}$, $(\dot{m}_{l,r})$	$p_{l,r}$, $T_{l,r}$ $(\dot{m}_{l,r})$
Throttle	$p_{l,r}$, T_L	$\dot{m}_{l,r}$, T_r
Volume	p_n, T_n, $\dot{m}_n$	p_n,T_n

Table 2.1: Summary of obtained and emitted information by the single components at each time step

Chapter 3

Numerical Results

In this chapter the following numerical tests on *DEOS* , on single components and on combinations of components are discussed:

- values for the speed of sound calculated from *DEOS* have been compared to literature data,
- the pipe has been tested by a shock tube test according to [Sod, 1978],
- the influence of a periodical change in size of a volume on temperature and pressure are shown,
- two volumes with different initial pressures have been connected via a throttle until pressure equilibrium is attained,
- two volumes with different initial pressures have been connected via a pipe leading to a balancing action.

3.1 Speed of sound

Since *DEOS* are the basis for every further calculation, they have been tested first. The isentropic speed of sound $c = \sqrt{\left(\frac{\partial \rho}{\partial p}\right)_s}$ is part of the Eigenvalues from the Jacobian of the flux function, see appendix I. Thus values for the speed of sound resulting from *DEOS* have been compared to values of the speed of sound according to equation (3.1)(see [Kolev, 2007]) in table 3.1

$$c = \sum_{i=1}^{3} \sum_{j=1}^{5} B_{ij} \left(\frac{p}{p_{ref}}\right)^{j-1} \left(\frac{T}{T_{ref}}\right)^{i-1} c_{ref}, \tag{3.1}$$

with the pressure $p_{ref} = 1$ Pa, the temperature $T_{ref} = 1$ K, the velocity $c_{ref} = 1\ \frac{\mathrm{m}}{\mathrm{s}}$ defining the system of units and with the dimensionless coefficient matrix B_{ij}:

$$B = \begin{pmatrix} 2226.4926 & 2.27318\ 10^{-6} & 2.75574\ 10^{-15} & 3.41172\ 10^{-22} & -1.74367\ 10^{-30} \\ -2.68172 & 3.79909\ 10^{-9} & -8.17983\ 10^{-17} & -1.65536\ 10^{-24} & 9.50961\ 10^{-33} \\ -0.00103 & 1.77949\ 10^{-11} & 6.4506\ 10^{-20} & 2.19744\ 10^{-27} & -1.29278\ 10^{-35} \end{pmatrix}.$$

While for high pressures and high temperatures the values from both approximations are in good agreement, the lower pressure and lower temperature regions show notable differences. The largest deviation of values calculated using *DEOS* from Kolev's approximations is 18.39%, for the case of pressure $p = 1$ bar and temperature $t = 380$ K.

Pressure [bar]	Temperature [K]	Kolev's speed of sound $[\frac{m}{s}]$	*DEOS* speed of sound $[\frac{m}{s}]$
2000	380	1796.2	1793.9
2000	290	1965.2	1989.2
1000	380	1527.0	1373.8
1000	290	1732.5	1726.2
500	380	1329.2	1300.2
500	290	1572.2	1655.4
1	380	1059.3	1298.1
1	290	1362.7	1621.3

Table 3.1: Comparison of values of velocity of sound calculated with (3.1) on the one hand, and calculated by the eigenvalues of (2.21) using *DEOS* on the other.

3.2 Shock Tube

The pipe has been tested with one of the standard tests in fluid dynamics, the shock tube (see references [Sod, 1978], [LeVeque, 2004], [Toro, 2009], [Guardone and Vigevano, 2001]). Initially the fluid has two different thermodynamical states on either side of an interface, which is located in the middle of the pipe. The initial state of the fluid is specified by $p_l = 1000$ bar on the left side of the interface and $p_r = 100$ bar on the right side. The fluid is assumed to be initially at rest and the fluid in the whole pipe has a temperature of $T = 290$ K. Therefore the density is different in the left and the right side of the interface (see Figure 3.1). The physical properties of the cladding pipe are given by the length of $l = 1$ m, the diameter of $d = 0.01$ m, a wall-thickness of $d_w = 0.002\ m$ and a thermal conductivity of $\lambda_h = 45\ \frac{\mathrm{W}}{\mathrm{m\ K}}$ similar to the thermal conductivity of stainless steal. The external temperature is assumed to have a fixed value of $T_{ext} = 290$ K. When this interface is removed, the fluid evolves in such a way that four states appear. Shortly after the removal these waves are not fully developed yet, but one can see the velocity of the fluid growing up to a certain value, depending amongst others on the pressure difference between both sides. Also the temperature increases on the right side, where the pressure increases, and temperature decreases on the left side where the pressure decreases, see figure 3.2. After 0.075 milliseconds the density shows a division into four different states,

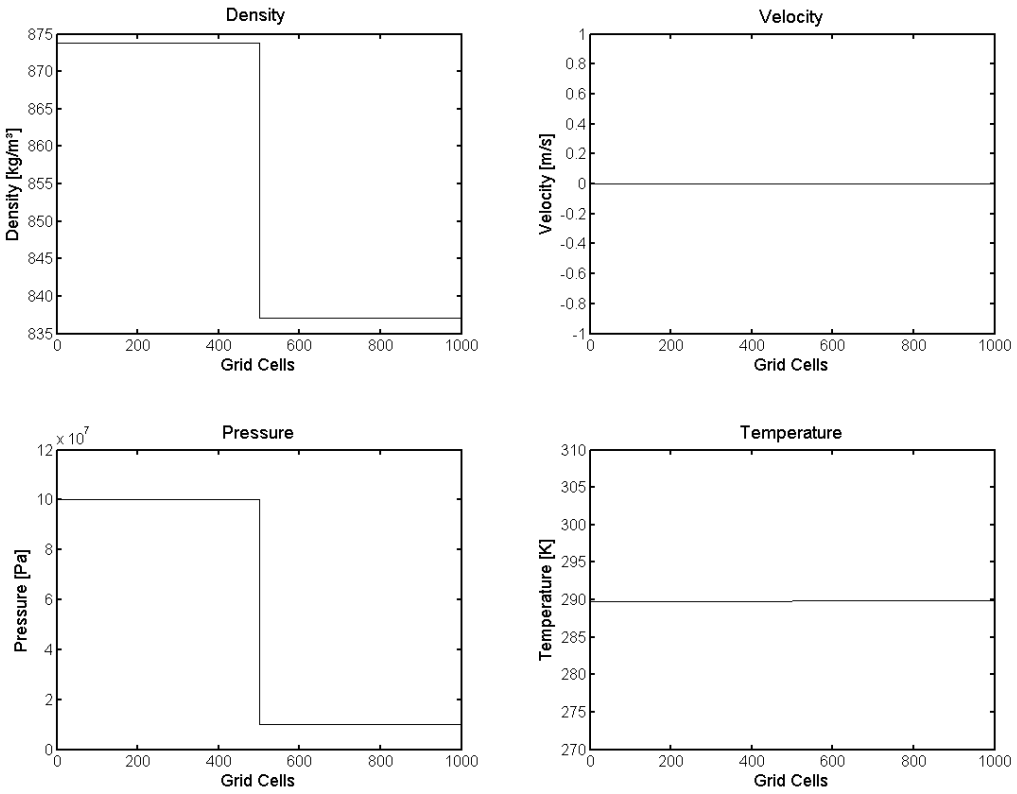

Figure 3.1: Initial conditions for the tested Shock Tube at $t = 0$ s. From the upper left to the lower right diagram there is shown the density, velocity, pressure and temperature over the length of the pipe, which is discretized by 1000 grid cells.

see figure 3.3. Each state is separated by one of three elementary waves. Starting from the left the rarefaction wave (often called rarefaction fan) separates the high density level from an intermediate level. Then the contact discontinuity divides the intermediate density region into two regions with slightly different densities. Then the shock wave separates the intermediate region from the low density region. While the rarefaction wave and the shock wave propagate with the speed of sound the contact discontinuity propagates with the velocity of the fluid. After 0.225 milliseconds the rarefaction fan and the shock wave have almost reached the ends of the pipe, see 3.4. To avoid influences from the boundary conditions the simulated time interval ended at this time. The time evolution of the fluid in the pipe, which was discretized using 1000 grid cells and a Courant Friedrichs Lewy -condition[1] of $CFL = 0.1$, can be found in a sequence of four figures 3.1, 3.2, 3.3, 3.4.

To calculate the transient solution to the shock tube problem, one of several solvers for ordinary differential equations (ode's) available in Matlab Simulink, had to be used for evaluating the change of the state vector Q over time (see (2.45). The ode solvers are named after the

[1] a necessary condition for convergence while solving certain partial differential equations numerically, see [Toro, 2009], [LeVeque, 2004]

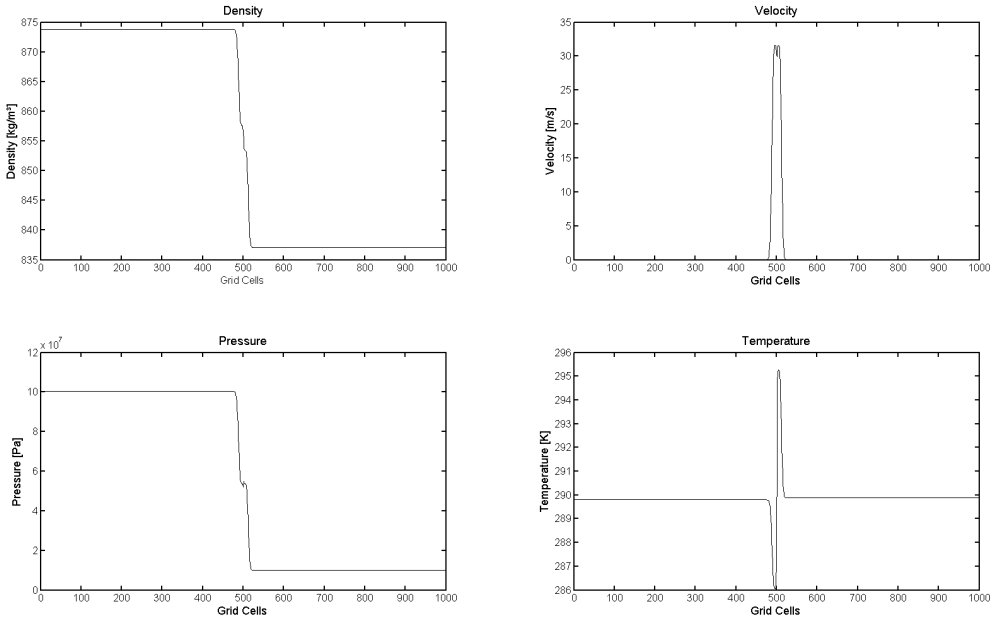

Figure 3.2: Solution for the shock tube at the time $T = 1.5\ 10^{-6}$ s after removal of interface. From the upper left to the lower right diagram, density, velocity, pressure and temperature are shown over the length of the pipe.

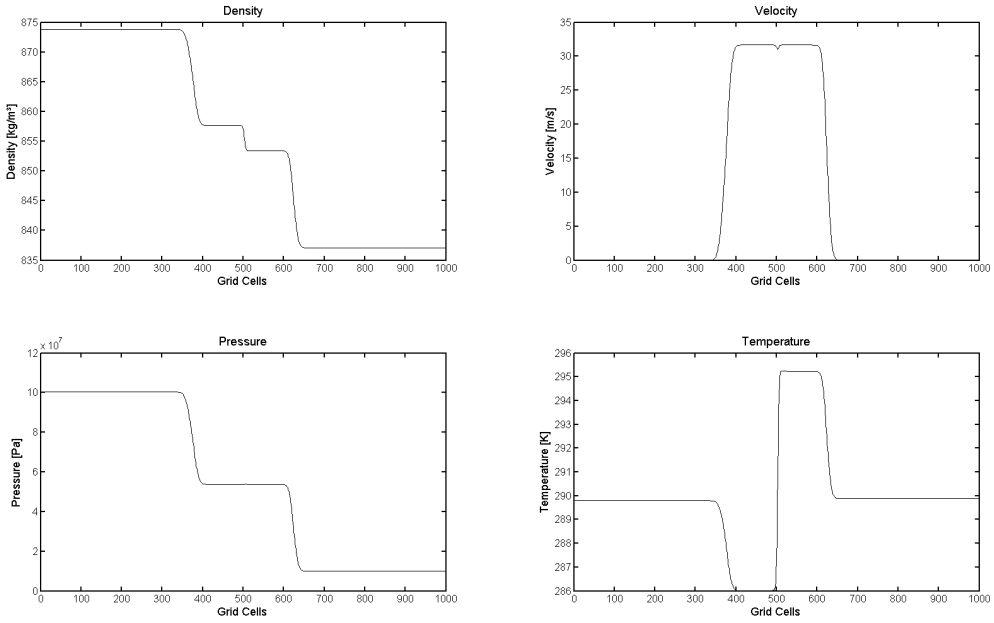

Figure 3.3: Solution for the shock tube at the time $T = 7.5\ 10^{-5}$ s after removal of interface.From the upper left to the lower right diagram, density, velocity, pressure and temperature are shown over the length of the pipe.

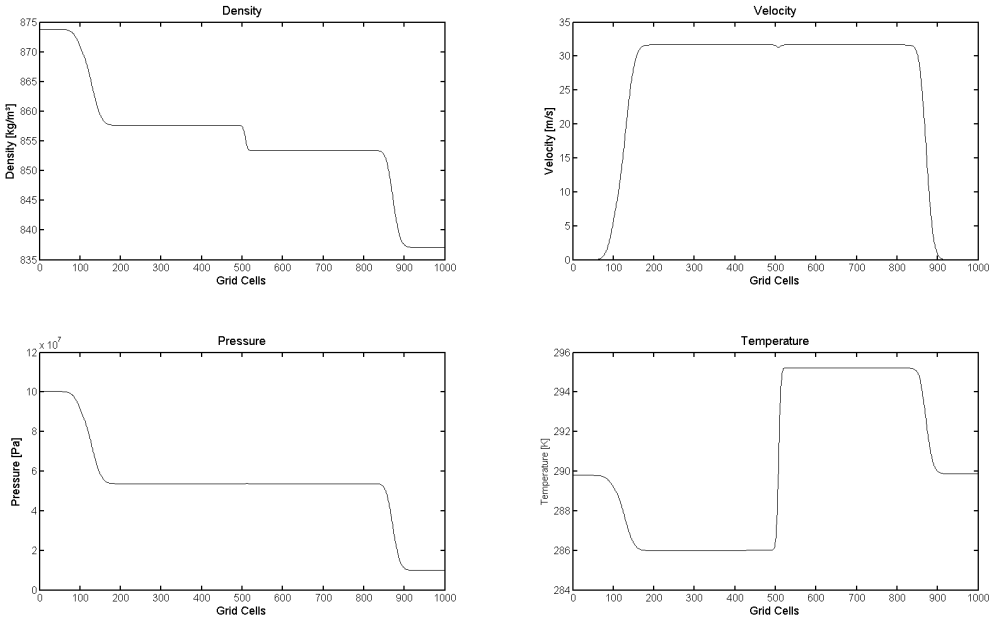

Figure 3.4: Solution for the shock tube at the time $T = 2.25\ 10^{-4}$ s after removal of interface.From the upper left to the lower right diagram, density, velocity, pressure and temperature are shown over the length of the pipe.

accuracy of the method. The available solvers using fixed timesteps are: ode1 (Euler's Method), ode2 (Heun's Method), ode3 (Bogacki-Shampine Formula), ode4 (Fourth-Order Runge-Kutta Formula) and ode5 (Dormand-Prince Formula). Literature on these solvers can be found in the Matlab manual or in [Shampine and Reichelt, 1997]. In order to rate which of these solvers is the best choice for this problem, the CPU time and the quality of the results are taken into account. Table 3.2 and Figure 3.5 show that solvers with low accuracies are sufficient accurate for this problem, because the results from the different solvers can hardly be distinguished, but the CPU time is significantly less for lower accurate solvers. Note that this evaluation only refers to simulation of the pipe alone, and not for systems containing other components.

Solver	Method	Order of accuracy	CPU time [min]
ode1	Euler	1	0.13144
ode2	Heun	2	0.22274
ode3	Bogacki - Shampine	3	0.30767
ode4	Runge - Kutta	4	0.39036
ode5	Dormand - Prince	5	0.56155

Table 3.2: CPU time of is shown for the shock tube with 200 grid cells and a fixed solver timestep of$\Delta t = 7.5\ 10^{-7}$. From the upper left to the lower right diagram, density, velocity, pressure and temperature are shown over the length of the pipe.

In order to dissolve shock and rarefaction waves, the amount of grid cells, used in the pipe,

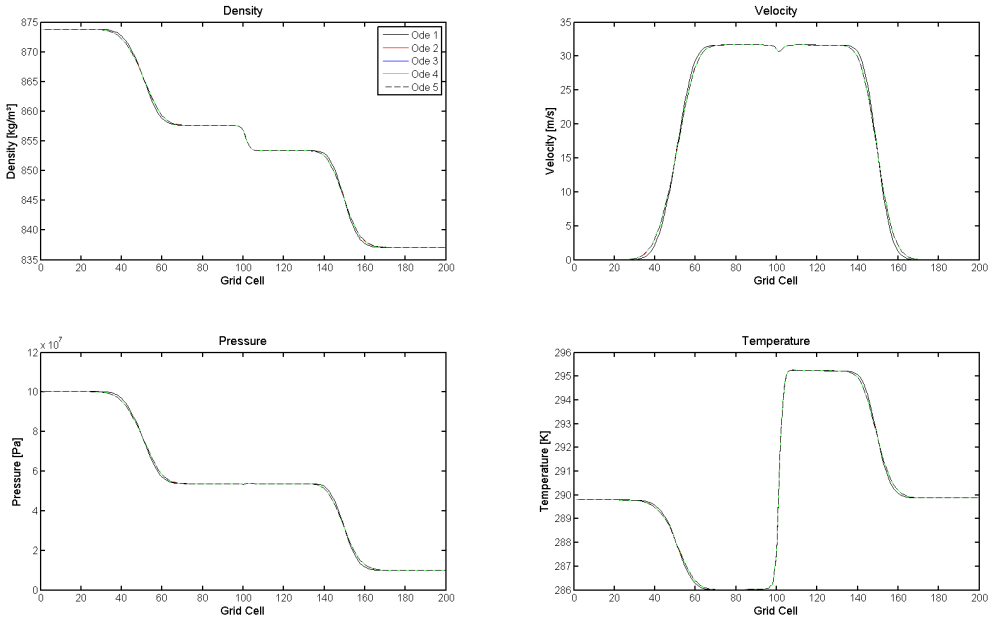

Figure 3.5: Results for shock tube with 200 grid cells, using different solvers in Matlab Simulink, at physical time $T = 1.5\ 10^{-4}$ seconds after release are shown. From the upper left to the lower right diagram, density, velocity, pressure and temperature are shown over the length of the pipe.

is of great importance. On the one hand the CPU time grows fast for an increasing number of grid cells (see Table 3.3). On the other hand, low numbers of grid cells lead to degeneration of the shock and rarefaction wave as well as degeneration of the contact discontinuity. The waves start to smear out as can be seen in Figure 3.6.

Amount of Cells	Used Timestep Δt	CPU time [min]
50	$2.4\ 10^{-6}$	0.048717
100	$1.2\ 10^{-6}$	0.074207
200	$6\ 10^{-7}$	0.15761
500	$3\ 10^{-7}$	0.6206
1000	$1.5\ 10^{-7}$	2.35630

Table 3.3: Influence of amount of grid cells on CPU time

3.3 Compressor

Here the volume has been tested by simulating the fluid in a cylinder, which gets compressed and diluted by a piston, that moves periodically with a frequency of $f = 50$ Hz. The ratio between the minimum and maximum size of the volume $\frac{V_{min}}{V_{max}} = 96\ \%$ and the minimum size of

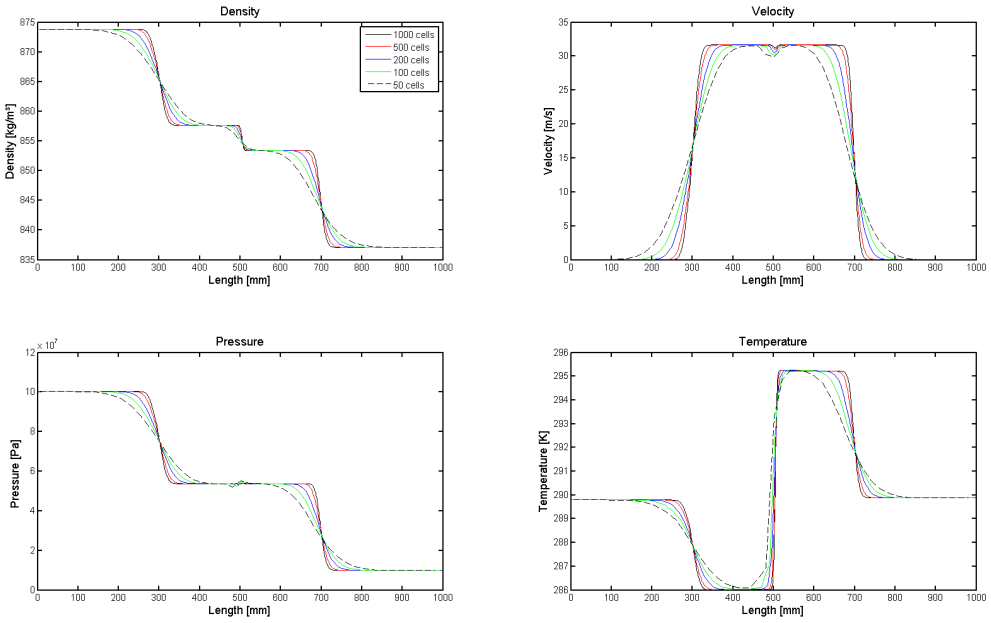

Figure 3.6: Results for shock tube test using different amounts of grid cells, and using the 'ode4' solver, are presented at physical time of $T = 1.2\ 10^{-4}\ s$ after release. From the upper left to the lower right diagram, density, velocity, pressure and temperature are shown over the length of the pipe.

the volume of $V_{min} = 0.001$ m^3. Thus the pressure raises from $p_{min} = 156$ bar up to $p_{max} = 2148$ bar during compression. The temperature raises from $T_{min} = 303$ K up to $T_{max} = 321$ K during the phase of compression.

3.4 Volume- Throttle- Volume

Similar to the shock tube test, this test is also about two different initial states, that lead to a transient action of the fluid. But here two volumes of the same size $V_1 = V_2 = 0.001$ m^3 have different initial pressures ($p_1 = 2000$ bar and $p_2 = 150$ bar) and since they have the same temperatures ($T_1^{ini} = T_2^{ini} = 313.15$ K) they also have different densities. The two volumes are connected via a throttle with an obstruction diameter of $d = 0.01$ m. Due to the pressure difference between both sides of the throttle, fluid is forced through the obstruction until the pressure in both volumes is balanced. The time dependent behavior of the fluid in the two volumes and in the throttle is shown in figure 3.8. For the described settings, pressure balance is reached shortly after 0.01 seconds. Note that the increase of fluid temperature in the second volume is not only a result of the raising pressure in this volume, but also because the diesel fuel heats up while passing the throttle.

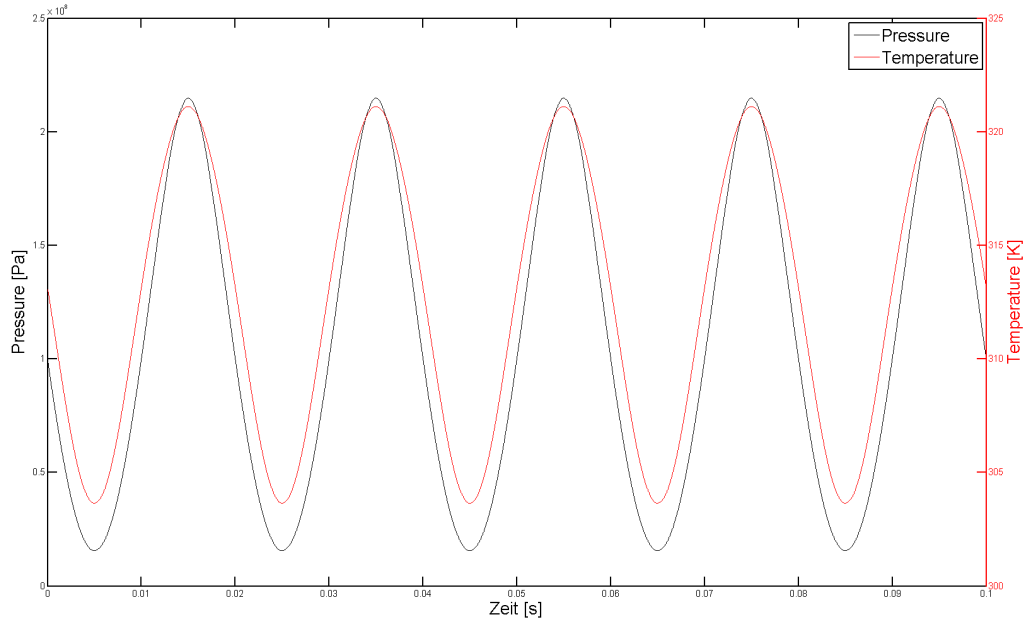

Figure 3.7: Pressure and temperature of the fluid in a cylinder with a moving piston are shown over a time interval of $\Delta t = 0.1$ s. The piston compresses and dilutes the fluid in a periodical way, with a frequency of $f = 50$ Hz.

3.5 Volume- Pipe- Volume

In this test again two volumes of the same size with different initial pressures, that are connected via a pipe, are analyzed. A similar test for one-dimensional unsteady flow procedures can be found in [Davis and Campbell, 2007]. The size of the volumes has been $V_1 = V_2 = 0.001$ m^3 and the initial pressures for this test have been $p_1 = 1250$ bar and $p_2 = 750$ bar. The pipe, which is discretized into 50 grid cells, has been $l = 0.1$ m long with an inner diameter of $d = 0.01$ m. The cladding material is assumed to be a stainless steel with a wall thickness of $d_w = 0.002$ m and a thermal conductivity of $\lambda_h = 45 \frac{\mathrm{W}}{\mathrm{m\ K}}$. The system is assumed to be initially in thermal equilibrium with the surrounding heat bath $T_1 = T_2 = T_{ext} = 313.15$ K, where the subindices 1 and 2 denote the temperatures in the volumes. The pressure difference between the volumes forces the fluid through the pipe. The quality of the transient action that occurs from these initial conditions is different to the previous test. Instead of clearing the initial pressure difference without any oscillations, now an oscillating state appears, seen figure 3.9. The frequency of the oscillation, which lies around $f \approx 600$ Hz, is much lower than the frequency of waves traveling through the pipe, which would lie around $f_{waves} \approx 18000$ Hz. The oscillation is not perpetual but slowly fading away until pressure balance is reached. The decay time of the oscillation is estimated from the change in amplitude to lie between one and two seconds.

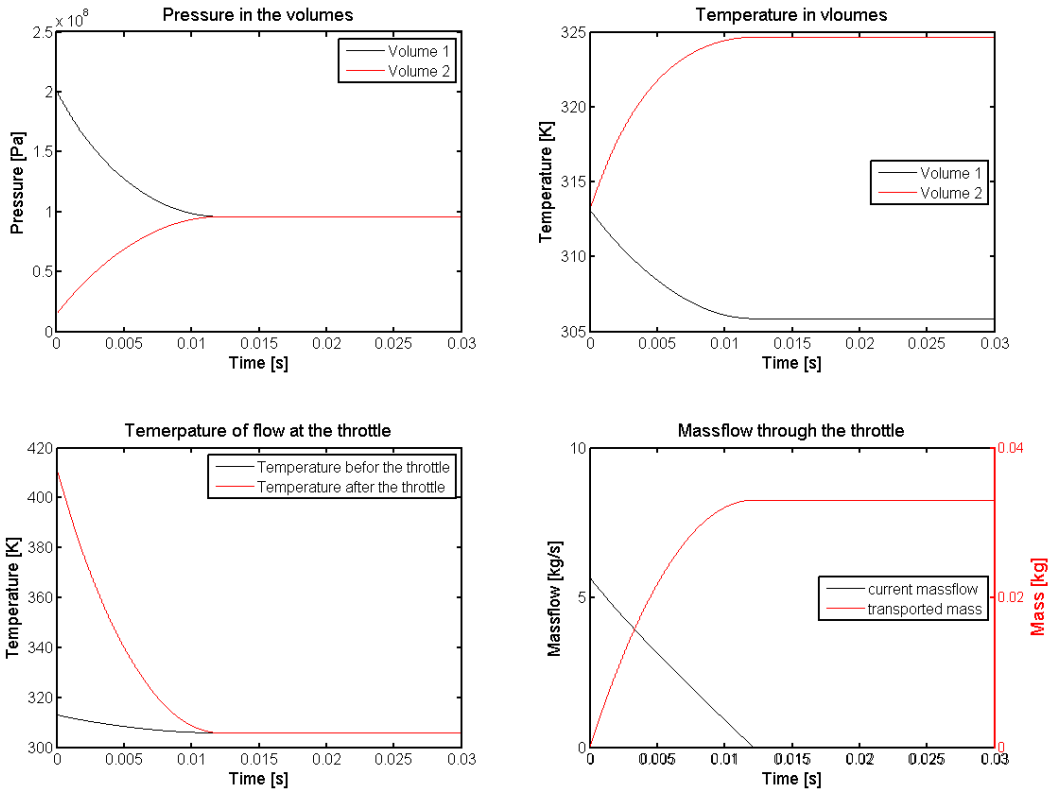

Figure 3.8: Balancing process of two vessels with different starting pressures ($p_1 = 2000$ bar, $p_2 = 150$ bar) and equal temperature($T_1 = T_2 = 313.15$ K), that are connected through a throttle with an obstruction diameter of $d = 0.01$ m. In the upper left and upper right diagram the pressure and the temperature in both volumes is shown. In the lower left diagram the temperature of the fluid into and out of the throttle can be found. In the lower right diagram the current mass flow on the one hand, and the total mass transported through the throttle on the other hand, can be seen.

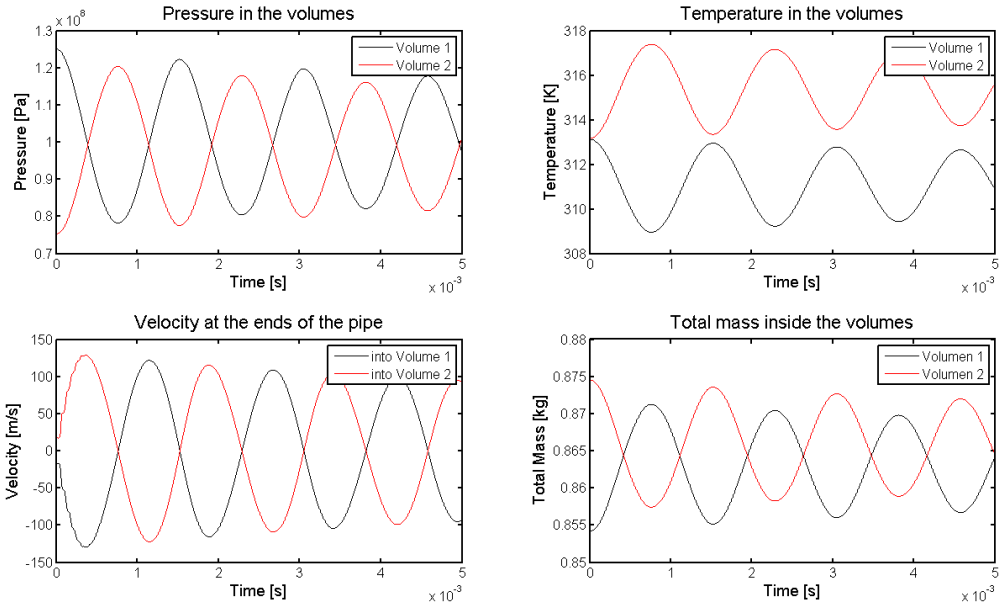

Figure 3.9: Oscillation of fluid parameters due to a initial value problem for two vessels connected via one pipe is shown. The transient development of the pressure and the temperature inside the vessels are shown in the upper left and upper right diagram. In the lower left diagram the change in velocity at both ends of the pipe over time can be seen. The lower right diagram shows that the mass in both vessels is oscillating.

Chapter 4

Discussion

The goal of this work was to create a simulation tool for analyzing fuel injection systems within Diesel engines. A fuel injection system can be seen as a hydrodynamic network out of pipes, throttles and volumes. Therefore these three components have been discussed and have been tested in different numerical tests. Also equations of state for liquid Diesel fuel have been presented, valid in a range from 1 bar up to 2500 bar in pressure and from 263.15 K up to 393.15 K in temperature.

The equations of state have been derived from measurements of the density $\rho = \rho(p, T)$ as a function of pressure p and temperature T and from measurements of the isobaric heat capacity $c_p^0(T) = c_p(p_0, T)$as a function of temperature T at a fixed pressure p_0. It is possible to use other thermodynamic properties to derive a consistent pair of state equations. We tried to derive a pair of state equations from the density $\rho = \rho(p, T)$ and the speed of sound $c^0(T) = c(p_0, T)$ as a function of temperature and with a fixed pressure, but the resulting values for the isobaric heat capacity turned out to differ with literature data. So we chose to use the density and the isobaric heat capacity, what turned out to deliver useful results. The velocity of sound resulting from this state equation is in good agreement with the approximation from the book [Kolev, 2007] for high pressures and high temperatures. The deviations in the lower pressure regions were accepted in order to stick with a inherently consistent equation of state, which is not available in Kolev's book [Kolev, 2007].

It was necessary to have a consistent state equation for using Roe's method to solve the Euler equations. Thus the flow in the pipe was assumed to be quasi one dimensional and inviscid, due to typically low velocities that occur in fuel injection systems. For the linearization procedure of Roe [Roe, 1981] an intermediate pressure $\hat{p}$ and an intermediate temperature $\hat{T}$ have to be found, which satisfy the conditions (2.52) and (2.53). Those conditions have been deduced assuming a pressure function $p = p(E^i, \rho)$ depending on the total internal energy E^i and on the density ρ, according to [Guardone and Vigevano, 2001]. The Euler equations have been extended with a source term. Considering that the pipe is connected to a heat bath, the temperature of the fluid can change because of heat conduction through the wall of the pipe. In the numerical results however, this effect was not of importance, because of the short time scales in the tests of only

up to 5 ms. In the shocktube test an analysis of the influence of grid cells has been performed, showing that waves tend to smear out according to the number of cells used, see figure 3.6. Since computational time raises with the number of cells (see table 3.3), it is up to the user of the simulation tool to decide, weather the high accurate but slow model is better than the low accurate fast one, or not. The test of the two volumes connected via a pipe has shown an oscillation in thermodynamic properties in both volumes. This oscillation only slowly fades away. Since no heat conduction inside the fluid is taken into account, the resulting state in the volumes have different temperatures. In order to improve the pipe heat conduction and friction should be added to the model. Therefore the source term vector (2.56) has to be changed. A further improvement of the pipe to take changes in cross section into account, would also be useful for may applications.

The whole simulation tool was implemented in Matlab Simulink 2008b. To reduce simulation time all embedded Matlab functions used in the Simulink model should be replaced by pre-implemented Simulink blocks.

Since the main interest of this work was to analyze the temperature behavior of liquid Diesel fuel, it is highly recommended to validate not only the equations of state but also the assumed physical behavior of the fluid in the single components by experiments measuring the temperature of the fluid. Due to the Joule-Thompson coefficient the Diesel fuel heats up, while passing a throttle, depending on the pressure drop. Since in the injector the pressure of the fluid drops from 2000 bar to ~ 150 bar, the change in temperature can be up to temperatures where Diesel starts to evaporate (Diesel starts to evaporate at temperature of $T = 390K$ [Kolev, 2007]), see figure 3.8.

The numerical results indicate that the presented methods are capable to simulate the flow of liquid Diesel fuel in Diesel injection systems, but experimental validation is highly recommended.

Part I

Appendix

Jacobian of the Euler flux function

In this section we want to analyze the Jacobian of the flux function from the Euler equations using a general equation of state. The only restriction for this general state equation is, that the described media is a pure substance. As mentioned before pure substances can be defined by two independent state variables [Schneider and Haas, 2004].
The Euler equations in conserved form can be written as

$$\vec{q}_t + f(\vec{q})_x = 0, \tag{1}$$

using the state vector $\vec{q}$ of conserved variables, or more precisely the Euler equations can be written as

$$\frac{\partial}{\partial t}\begin{bmatrix}\rho\\ M\\ E\end{bmatrix} + \frac{\partial}{\partial x}\begin{bmatrix}M\\ \frac{M^2}{\rho}+p\\ \frac{(E+p)M}{\rho}\end{bmatrix} = 0. \tag{2}$$

The Jacobian $J = \frac{\partial f}{\partial q_i}$ of the flux function $f(\vec{q})$ denotes to

$$J = \begin{bmatrix} 0 & 1 & 0\\ -\frac{M^2}{\rho^2}+\frac{\partial p}{\partial \rho} & 2\frac{M}{\rho}+\frac{\partial p}{\partial M} & \frac{\partial p}{\partial E}\\ \frac{-(E+p)M}{\rho^2}+\frac{M}{\rho}\frac{\partial p}{\partial \rho} & \frac{E+p}{\rho}+\frac{M}{\rho}\frac{\partial p}{\partial M} & \frac{M}{\rho}(1+\frac{\partial p}{\partial E}) \end{bmatrix}. \tag{3}$$

The Euler equations can be transformed to new coordinates $Q^{(new)} = (\rho, M, S)$, where $S = \rho s$ is the entropy. In the case of flow without friction or heat conduction, this flow is considered to be isentropic, and the Euler equations can be rewritten as

$$\frac{\partial}{\partial t}\begin{bmatrix}\rho\\ M\\ S\end{bmatrix} + \frac{\partial}{\partial x}\begin{bmatrix}M\\ \frac{M^2}{\rho}+p\\ S\frac{M}{\rho}\end{bmatrix} = 0 \tag{4}$$

(see [Steinrück, 2008]). Now the equation of state for pressure $p = P(\rho, s) = P(\rho, S\frac{1}{\rho})$ has to be inserted and in the course of that the velocity of sound gets introduced

$$c^2 = \left(\frac{\partial P}{\partial \rho}\right)_S. \tag{5}$$

The specific entropy can be written as

$$s = S\frac{1}{\rho} = s(\rho, e) = s(\rho, \frac{E}{\rho} - \frac{M^2}{2\rho^2}), \tag{6}$$

due to the basic assumptions for the general state equation. Therefore the derivatives of the pressure function can be calculated to

$$\left(\frac{\partial P}{\partial \rho}\right)_S = \left(\frac{\partial P}{\partial \rho}\right)_S - \left(\frac{\partial P}{\partial s}\right)_\rho \frac{S}{\rho^2} = c^2 - \left(\frac{\partial P}{\partial s}\right)_\rho \frac{S}{\rho^2}, \tag{7}$$

and

$$\left(\frac{\partial P}{\partial S}\right)_\rho = \left(\frac{\partial P}{\partial s}\right)_\rho \frac{1}{\rho}. \tag{8}$$

The Jacobian $J^{(S)}$ of the flux function in the new coordinates denotes to

$$J^{(S)} = \begin{bmatrix} 0 & 1 & 0 \\ -\frac{M^2}{\rho^2} + c^2 - \frac{S}{\rho^2}\left(\frac{\partial P}{\partial s}\right)_\rho & 2\frac{M}{\rho} & \left(\frac{\partial P}{\partial s}\right)_\rho \frac{1}{\rho} \\ -S\frac{M}{\rho^2} & \frac{S}{\rho} & \frac{M}{\rho} \end{bmatrix}. \tag{9}$$

Inserting an expression for the velocity $u = \frac{M}{\rho}$ and using an expression for $\left(\frac{\partial P}{\partial s}\right)_\rho = \frac{\rho c^2}{c_p} T\beta$ (see [Schneider and Haas, 2004]) the Jacobian get the form

$$J^{(S)} = \begin{bmatrix} 0 & 1 & 0 \\ -u^2 + c^2(1 - \frac{T\beta s}{c_p}) & 2u & \frac{c^2 T\beta}{c_p} \\ -su & s & u \end{bmatrix}. \tag{10}$$

Now the Jacobian gets transformed back into the conserved system $Q = Q(\rho, M, E)$ using the transformation matrix $TM = \frac{\partial Q(\rho,M,S)}{\partial Q(\rho,M,E)}$

$$TM = \begin{pmatrix} 1 & 0 & 0 \\ 0 & 1 & 0 \\ \frac{\partial S}{\partial \rho} & \frac{\partial S}{\partial M} & \frac{\partial S}{\partial E} \end{pmatrix} \tag{11}$$

Due to the chain rule for differentiation the derivations of the entropy with respect to the conserved variables can be calculated using the definition (6):

$$\frac{\partial S}{\partial \rho} = s + \rho \left(\frac{\partial s}{\partial \rho}\right)_e + \rho \left(\frac{\partial s}{\partial e}\right)_\rho \left(-\frac{E}{\rho^2} + \frac{M^2}{\rho^3}\right), \tag{12}$$

$$\frac{\partial S}{\partial M} = \rho \left(\frac{\partial s}{\partial e}\right)_\rho \left(-\frac{M}{\rho^2}\right), \tag{13}$$

$$\frac{\partial S}{\partial E} = \left(\frac{\partial s}{\partial e}\right)_\rho. \tag{14}$$

Using the Maxwell relations

$$\left(\frac{\partial s}{\partial e}\right)_\rho = \frac{1}{T} \tag{15}$$

and

$$\left(\frac{\partial s}{\partial \rho}\right)_e = -\frac{p}{T\rho^2}, \tag{16}$$

we can rewrite the transformation matrix

$$TM = \begin{pmatrix} 1 & 0 & 0 \\ 0 & 1 & 0 \\ s - \frac{1}{T}(h - \frac{u}{2}) & -\frac{u}{T} & \frac{1}{T} \end{pmatrix} \tag{17}$$

with it's inverse T^{-1}

$$TM^{-1} = \begin{pmatrix} 1 & 0 & 0 \\ 0 & 1 & 0 \\ h - sT - \frac{u}{2} & u & T \end{pmatrix} \tag{18}$$

Now the transformation of the Jacobian Matrix from entropy system back to conserved system can written as

$$J^{(E)} = TM^{-1}J^{(S)}TM = \begin{pmatrix} 0 & 1 & 0 \\ \frac{-2c_pu^2+c^2(2c_p+\beta(-2h+u^2))}{2c_p} & (2-\frac{\beta c^2}{c_p})u & \frac{\beta c^2}{c_p} \\ \frac{u(-c_p(2h+u^2)+c^2(2c_p+\beta(-2h+u^2)))}{2c_p} & h+\frac{(-2\beta c^2+c_p)u^2}{2c_p} & u+u\frac{\beta c^2}{c_p} \end{pmatrix} \tag{19}$$

Similar to the Eigenvalues for an ideal gas the Eigenvalues for a general equation of state (λ_i) turn out to be

$$\lambda_1 = u - c,\ \lambda_2 = u,\ \lambda_3 = u + c \tag{20}$$

with their associated Eigenvectors r_i

$$r_1 = \begin{pmatrix} 1 \\ u - c \\ H - cu \end{pmatrix},\ r_2 = \begin{pmatrix} 1 \\ u \\ H - \frac{c_p}{\beta} \end{pmatrix}, r_3 = \begin{pmatrix} 1 \\ u + c \\ H + cu \end{pmatrix} \tag{21}$$

To proof this statement thermodynamic properties of an ideal gas can be inserted into (21). For an ideal gas the isothermal expansion coefficient is

$$\beta = \frac{1}{T} \tag{22}$$

and the specific entropy can be written as

$$h = c_p\ T = H - \frac{u^2}{2} \tag{23}$$

Therefore the eigenvector r_2, which is the only one differing from the eigenvectors of an ideal gas,

$$r_2 = \begin{pmatrix} 1 \\ u \\ H - \frac{c_p}{\beta} \end{pmatrix} = \begin{pmatrix} 1 \\ u \\ \frac{u^2}{2} \end{pmatrix} \tag{24}$$

turns out to be the same as for an ideal gas, see [LeVeque, 2004].

Bibliography

[BMW, 2006] BMW (2006). Baustein: Grundlagen motorentechnik. www.pinoe-hl.ac.at/arge/ahsph/steyr2007/5-motorelektrik.pdf, München, Germany.

[Chorin and Marsden, 1993] Chorin, A. J. and Marsden, J. (1993). *A Mathematical Introduction to Fluid Mechanics*. Springer, New York.

[Davis and Campbell, 2007] Davis, R. and Campbell, B. (2007). Quasi-one-dimensional unsteady-flow procedure for real fluids. *AIAA*, 45(10):2422–2428.

[Elmqvist, 2003] Elmqvist, H. e. a. (2003). Object-oriented modeling of thermo-fluid systems. *Proceedings of the* 3^{rd} *International Modelica Conference*.

[Guardone and Vigevano, 2001] Guardone, A. and Vigevano, L. (2001). Roe linearization for the van der waals gas. *J. Comput. Phys.*, 175:50–78.

[Hudson, 2006] Hudson, J. (2006). A review on the numerical solution of the 1d euler equations. MIMS EPrint 2006.9, Manchester, UK.

[Kolev, 2007] Kolev, N. I. (2007). *Multiphase Flow Dynamics 3*. Springer, Berlin - Heidelberg.

[Landau and Lifshitz, 1987] Landau, L. and Lifshitz, E. (1987). *Fluid Mechanics*. Pergamon Press.

[Leonhard, 2009] Leonhard, R. e. a. (2009). Druckübersetztes common - rail - system für nutzfahrzeuge. *MTZ*, 70:368–375.

[Levenberg, 1944] Levenberg, K. (1944). A method for the solution of certain problems in least squares. *Quart. Appl. Math.*, 2:164–168.

[LeVeque, 2004] LeVeque, R. J. (2004). *Finite Volume Methods for Hyperbolic Problems*. Cambridge University Press.

[Mollenhauer, 2002] Mollenhauer, K. (2002). *Handbuch Dieselmotoren*. Springer.

[Parche, 2010] Parche, M. e. a. (2010). Bosch 2000/2200 bar common rail systems for commercial vehicles. 31. internationales wiener motorensymposium, Robert Bosch GmbH, Stuttgart.

[Predelli, 2010] Predelli, O. e. a. (2010). Continuous injection rate-shaping for passenger-car diesel engines - potential, limits and feasibility. 31. internationales wiener motorensymposium, Ingenieurgesellschaft Auto und Verkehr GmbH, Berlin.

[Roe, 1981] Roe, P. (1981). Approximate riemann solvers, parameter vectors and difference schemes. *J. Comput. Phys.*, 43:357–372.

[Schneider and Haas, 2004] Schneider, W. and Haas, S. (2004). *Repetitorium Thermodynamik*. R. Oldenbourg, Wien - München.

[Shampine and Reichelt, 1997] Shampine, L. and Reichelt, M. (1997). The matlab ode suite. *SIAM J. Sci. Comput.*, 18(1):1–22.

[Sod, 1978] Sod, G. (1978). A survey of several finite difference methods for systems of nonlinear hyperbolic conservation laws. *J. Comput. Phys.*, 27:1–31.

[Steinrück, 2008] Steinrück, H. (2008). *Skriptum: Wärmeübertragung*. TU Wien.

[Toro, 2009] Toro, E. (2009). *Riemann Solvers and Numerical Methods for Fluid Dynamics*. Springer, Berlin - Heidelberg.

[White, 2006] White, F. (2006). *Fluid Mechanics. Sixth Edition*. McGraw-Hill int.